Supplementary Information for

Understanding the uptake of nanomedicines at different stages of brain cancer using a modular nanocarrier platform and precision bispecific antibodies

Zachary H. Houston[1,2,5], Jens Bunt[3], Kok-Siong Chen,[3,13], Simon Puttick[2,10], Christopher B. Howard[1,2,5,6,11], Nicholas L. Fletcher[1,2,5], Adrian V. Fuchs[1,2,5], Jiwei Cui[4,5,12], Yi Ju[4,5], Gary Cowin[1], Xin Song[1], Andrew W. Boyd[7,8], Stephen M. Mahler[2,11], Linda J. Richards[3,9], Frank Caruso[4,5], Kristofer J. Thurecht[1,2,5,6]*

[1] *Centre for Advanced Imaging, The University of Queensland, St Lucia, QLD 4072, Australia.*
[2] *Australian Institute for Bioengineering and Nanotechnology, The University of Queensland, St Lucia, QLD 4072, Australia.*
[3] *Queensland Brain Institute, The University of Queensland, St Lucia, QLD 4072, Australia*
[4] *Department of Chemical Engineering, The University of Melbourne, Parkville, VIC 3010, Australia*
[5] *ARC Centre of Excellence in Convergent BioNano Science and Technology, The University of Queensland, St Lucia, QLD 4072, Australia*
[6] *ARC Training Centre for Innovation in Biomedical Imaging Technology, The University of Queensland, St Lucia, QLD 4072, Australia*
[7] *Leukaemia Foundation Laboratory, QIMR-Berghofer Medical Research Institute, Herston, QLD 4006, Australia*
[8] *Department of Medicine, The University of Queensland, St. Lucia, QLD 4072, Australia*
[9] *The School of Biomedical Sciences, The University of Queensland, St. Lucia, QLD 4072, Australia*
[10] *Commonwealth Scientific and Industrial Research Organisation, Probing Biosystems Future Science Platform*
[11] *ARC Training Centre for Biopharmaceutical Innovation The University of Queensland, St Lucia, QLD 4072, Australia*
[12] *Key Laboratory of Colloid and Interface Chemistry of the Ministry of Education, School of Chemistry and Chemical Engineering, Shandong University, Jinan, Shandong 250100, China*
[13] *Brigham and Women's Hospital, Harvard Medical School, Boston, MA 02115, USA*

Table of Contents

Section 1 – Materials and Methods

All data in this paper was collected and analysed in accordance with the Minimum Information Reporting in Bio-Nano Experimental Literature (MIRIBEL) guidelines in order to maintain the best reporting of reproducible and reliable data.[63] The full checklist and comments with regards to the materials and analyses performed are outlined in Section 10 of the supplementary information. In the preparation of all materials and the execution of the experiment no unexpected or unusually high safety hazards were encountered.

S1.1 – Materials for sNP

2-aminoethyl methacrylate hydrochloride, trimethylamine (TEA), poly(ethylene glycol) monomethyl ether methacrylate 475 (PEGMA), ethylene glycol dimethacrylate (EGDMA), and azobis(isobutyronitrile) (AIBN) were all used as received from Sigma-Aldrich. 2-S-(4-Isothiocyanatobenzyl)-1,4,7-triazacyclononane-1,4,7-triacetic acid (NOTA-NCS) was used as received from Macrocyclics. Methanol (MeOH) and N-N-dimethylformamide (DMF) were used dry where applicable and of reagent grade quality. Milli-Q water (18.2 mΩ cm) was used throughout. Lipophlic Sephadex® size-exclusion media was purchased from Sigma-Aldrich and swelled according to the manufacturer's recommendation. PEGMA and EGDMA were filtered through basic alumina to remove radical inhibitors before use.

S1.2 – Materials for bNP

Tetraethyl orthosilicate (TEOS), cetyltrimethylammonium tosylate (CTAT), triethanolamine, hydrofluoric acid (HF; 48 wt %), and ammonium fluoride (NH_4F) were obtained from Sigma-Aldrich (Australia). 8-arm-PEG-NH_2 (40 kDa) and 8-arm-PEG-succinimidyl (NHS) ester (10 kDa) with a hexaglycerol core structure were purchased from JenKem Technology (China) and Creative PEGWorks (USA), respectively. MeCOSAR was synthesized by Brett M. Paterson and Paul S. Donnelly at the University of Melbourne.[14]

S1.3 – Synthesis of sNP

Both the Cy5-methacrylate monomer (Cy5-MA)[64] and the 4-cyano-4[(2-phenylethylsulfanylthiocarbony)sulfanyl pentanoic acid chain transfer agent (CTA)[65] have been previously reported and were prepared as published. The hyperbranched polymer (sNP) was prepared as previously reported,[64] but with the addition of a monomer for NOTA (NOTA-MA). Briefly, the hyperbranched polymer sNP was synthesised by adding; PEGMA (100 mg, 211 µmol), EGDMA (2.2 mg, 11.1 µmol), NOTA-MA (6.4 mg, 11.1 µmol), Cy5-MA (737 µg, 1.1 µmol), CTA (3.7 mg, 11.1 µmol), and AIBN (264 µg, 2.2 µmol) to a Schlenk tube. The reagents were dissolved in DMF (270 µL) and the solution was degassed with N_2 for 20 min, sealed and submerged in an oil bath at 80°C for 24 h. The resultant DMF solution was dried *in vacuo* and the crude product was purified *via* size exclusion chromatography using Sephadex® LH-20 as the stationary phase and isocratic MeOH as the mobile phase. Yield: 93.0 mg, 85%. The synthesis for the NOTA-MA monomer and characterisation is reported in the supplementary information (Supplementary, Section 7.1), as is the full characterisation data for the sNP polymer (Supplementary, Section 7.2). The pure product was then redissolved in Milli-Q water for conjugation to ^{64}Cu.

S1.4 – Synthesis of bNP

PEG hydrogel particles were prepared using 100 nm mesoporous silica (MS) templates as previously reported.[14] Briefly, MS particles (6 g) were washed with phosphate buffer (100 × 10^{-3} M, pH 8) and incubated in 8-arm-PEG-NH_2 solution (480 µL, 5 mg mL^{-1} in phosphate buffer) overnight with constant shaking. The particles were isolated by centrifugation (3000 g, 3 min) and washed thrice using phosphate buffer. The pellet was dispersed in 8-arm-PEG-NHS solution (400 µL, 2 mg mL^{-1} in phosphate buffer) and incubated for 2 h. The MS-templated PEG particles were labeled with MeCOSar-NHS Ester (5 µL, 1 mg mL^{-1} in DMSO) during the cross-linking step. After washing thrice with water, the MS-templated PEG particles were resuspended in water. The silica template was removed using 600 µL of 2 M HF/8 M NH_4F solution (pH 5). The resultant PEG particles (100 ± 9 nm diameter by TEM, n=100, Supplementary Section 8, 150 nm diameter as by super-resolution microscopy) were purified with a Zeba™ spin desalting column (40K MWCO) (Life Technologies, U.S.A.) and dispersed in Milli-Q water for ^{64}Cu labelling.

S1.5 – ^{64}Cu labelling of sNP and bNP

Stock solutions with known concentrations of sNP and bNP were incubated with ^{64}Cu at a 300-fold excess of the nanoparticle (sNP or bNP) in 0.1 M pH 5.5 Ammonium Acetate buffer. The sNP reaction was stirred for 45 minutes at room temperature, while the bNP reaction was stirred for 6 hours at 4 °C. Samples of each solution were taken and mixed 1:1 with 50 mM EDTA. 5 uL of each solution was spotted on TLC paper (Agilent iTLC-SG Glass microfiber chromatography paper impregnated with silica gel) and run with 50:50 H_2O:Ethanol. Plates were then imaged on a Carestream MSFX imaging system using a radioisotopic phosphor screen. Both sNP and bNP showed >95% labelling. Control experiments were conducted to monitor the elution behaviour of free ^{64}Cu and ^{64}Cu bound to EDTA (Supplementary, Figure S5.1) for quality control. The pure samples were then conjugated to the BsAb after radiolabelling as conjugation is optimised at physiological pH (7.4) as described below.

S1.6 – Preparation of EphA2 BsAb

BsAbs were expressed in Chinese hamster ovary CHO-S cells as previously described.[16] Briefly, genes encoding the BsAbs were synthesised by Geneart (Invitrogen). A 6×His motif (for affinity purification) and a c-Myc epitope (for detection by fluorescent αMyc Abs) were included at the N- and C-termini, respectively. The BsAb genes were cloned into a mammalian expression plasmid (pcDNA 3.1 (+), Invitrogen) using HindIII and NotI restriction sites. Plasmid DNA (2 µg mL^{-1}) was complexed with polyethylenimine-Pro (PolyPlus) in Opti-Pro serum free medium (Life Technologies) at a DNA (µg) to PEI (µL) ratio of 1:4 (w:v) for 15 min before transiently transfecting suspension adapted CHO-S cells (3 × 10^6 mL^{-1}). Cells were grown in chemically defined CHO medium (CD-CHO, Life Technologies) at 37 ˚C, 7.5 % CO_2 with shaking (130 rpm) for 6 h, before adding 7.5 % CD-CHO Efficient Feed A (Life Technologies), 7.5 % CD-CHO Efficient Feed B (Life Technologies) and 0.4 % anti-clumping agent (Gibco), and culturing at 32 ˚C, 7.5 % CO_2 with shaking for 7-14 days. Cells were cultured until their viability reduced below 50 % as measured by trypan blue exclusion. Following expression, BsAbs were purified by pelleting cells by centrifugation (5250 rcf, 30 min), filtering supernatant through a 0.22 µm membrane (Sartorius) and purifying with a 5 mL HisTrap excel column (GE Healthcare). BsAbs were eluted with 20 × 10^{-3} M sodium phosphate, 500 × 10^{-3} M sodium chloride and 500 × 10^{-3} M imidazole pH 7.4. Alternatively, a 5 mL Protein L column was used, with BsAbs eluted using 100 × 10^{-3} M glycine pH 3.0. Following buffer exchange and size exclusion chromatography as

described previously[44], BsAbs were filtered through 0.22 µm membranes and stored at 0.25-0.60 mg mL^{-1} in buffer containing 20 × 10^{-3} M sodium phosphate, and 500 × 10^{-3} M sodium chloride, pH 7.6.

S1.7 – Preparation of BsAb targeted sNP and bNP

The targeted sNP-EphA2 conjugate was prepared by mixing the ^{64}Cu labelled sNP and BsAb in a 3:1 (BsAb:sNP) molar ratio in PBS (1X) and were shaken continuously at 700 rpm (Eppendorf Thermomixer) at room temperature for 1 hour. The larger bNP-EphA2 conjugate was prepared by mixing the ^{64}Cu labelled bNP and BsAb in an 8:1 (BsAb:bNP) molar ratio in PBS (1X) and stirred continuously at 4 ˚C for 6 h. The resulting mixtures from both particles were directly injected into the mice without further purification.

S1.8 – PET-MRI Imaging

Anaesthetized mice, with a cannulated tail vein, were placed in a combined MRI/PET system, comprising a 300mm bore 7T ClinScan, running Siemens VB17, and removable PET insert containing 3 rings of 16 detector blocks with 15 × 15 LSO crystals (1.6 × 1.6 × 10mm) per block, at the centre of the magnet bore operating under Siemens Inveon Acquisition Workplace (IAW) (Bruker, Germany). A 23 mm ID mouse head MRI RF coil inside the PET ring was used to acquire mouse head images simultaneously with the PET acquisition.

For ^{64}Cu nanomedicine imaging mice were injected with approximately 5-6 MBq of ^{64}Cu labelled sNP or bNP, 50 µl Gadovist® and diluted with PBS (1X) to give a total volume of 200 µl. For all other scans not using radiotracers 50 µl of Gadovist® was diluted with 150 µl PBS (1X) to give a total volume of 200 µl. This volume was injected *via* a catheter inserted into the tail vein in a slow bolus injection. Where collected, dynamic PET data acquisition was performed for 60 min. Prior to injection, fast localizer images and a 3D T1 weighted volumetric interpolated breath-hold examination VIBE sequence was acquired. Dynamic MRI images were acquired with a Gradient echo FLASH sequence, with 3 slices acquired each 2 seconds interval. The PET acquisition (60 minutes) and dynamic MRI imaging was started simultaneously, a 2-3 min baseline period acquired and then the solution was injected. Following 15 min of dynamic MRI scanning, the T1 weighted VIBE was repeated, structural T2 weighted spin echo images acquired and a 3T T1 weighted VIBE_DIXON sequence acquired to generate a 3D T1 map.

The PET data was reconstructed using dedicated PET reconstructed software developed by the University of Tubingen for the PET insert. PET images with a matrix of 128X128X89 were reconstructed using the ordered-subset expectation maximization (OSEM2D) algorithm. MRI and PET datasets were aligned using IRW software (Siemens) using a transformation matrix generated using a phantom with known features.

S1.9 – Image Processing

All MRI images were acquired or using the ClinScan software mentioned above, and subtraction images were calculated using the built-in function. All images were exported as DICOMS from the ClinScan software and further processed and analysed with Osirix MD for the dynamic uptake, T1- and T2- weighted images as MRI alone (v 9.0.1). PET data and

resulting generated PET-MRI fusion maximum intensity projection images were prepared using Siemens Inveon Research Workplace software (v 4.2).

S1.10 – Data analysis

Data was aggregated in Microsoft Excel (Mac 2016, v 16.24) and basic mathematic calculations were done within the worksheets. All plots were made with GraphPad Prism 7 and all statistical analyses and area under curve measurements were done using the built-in functions. Calculations for radiotracer uptake are presented as percent injected dose per gram (%ID/g) and were calculated from the *in vivo* images using Siemens Inveon Research Workplace. Further information pertaining to data analyses can be found in their respective sections in the supplementary information.

S1.11 – Mouse model

All breeding and experiments were performed at the University of Queensland in accordance with the Australian Code of Practice for the Care and Use of Animals for Scientific Purposes and with approval from the University of Queensland Animal Ethics Committee. Gt(ROSA)26So$^{rtm14(CAG-tdTomato)Hze}$ 20023653 was crossed with Pten^{tm2MAK}; Rb1^{tm2Brn}; Trp53^{tm1Brn}; Tg(GFAP-cre/Esr1*,-lacZ)BSbk[11, 66-69] (alleles) and backcrossed six generations to latter mice to generate Gt(ROSA)26Sor$^{tm14(CAG-tdTomato)Hze}$; Pten^{tm2MAK}; Rb1^{tm2Brn}; Trp53^{tm1Brn}; Tg(GFAP-cre/Esr1*,-lacZ)BSbk (high grade glioma mouse model; HGG). Mice were maintained on a predominantly FVB/NJ background with contributions from 129/SV and C57Bl6. To induce Cre recombinase and thereby tumor formations, 20 mg/ml Tamoxifen (Sigma-Aldrich) dissolved in corn oil (Sigma-Aldrich) was injected intraperitoneal. Up to 200 mg/kg body weight was administered weekly for 3 consecutive weeks after postnatal day (P) 30 (range P30–44). Animal's health and welfare was monitored up to twice daily and animals were euthanized based on morbidity requirement.

S1.11 – Tissue collection, processing, and confocal microscopy

Mouse brains were fixed *via* transcardial perfusion or immersion fixation with 4% paraformaldehyde solution, as previously described.[70] Following post-fixation up to 10 days, the dissected brains were embedded in 3–4% w/v Difco Noble agar (Becton, Dickinson and Company, Sparks, MD) and sectioned coronally at 50 µm on a vibratome (Leica). The sections were then mounted onto SuperfrostPlus slides (Menzel-Gläser, Brunswick, Germany), and dried at room temperature until fully adherent. Sections were post-fixed with 4% w/v paraformaldehyde for 10 min and rehydrated with phosphate buffered saline (PBS) for 5 min prior to immunohistochemistry.

Fluorescence immunohistochemistry was conducted as previously described.[70] For the staining to test the specificity of EphA2 antibody, brain sections were antigen-retrieved in an antigen decloaking chamber (Biocare Medical, Concord, CA). The sections were heated to 125°C for 4 min at 15 psi in sodium citrate buffer (10 mM $C_6H_5Na_3O_7$. $2H_2O$, 0.05% v/v Tween 20 (Sigma-Aldrich) in MilliQ water, pH 6.0). Sections with and without antigen-retrieval on the slides were then washed in PBS for 5 min and incubated for 2 hr in blocking solution containing 10 % v/v normal donkey serum (Jackson ImmunoResearch Labs, West Grove, PA; Cat# 017-000-001), 0.9% v/v H_2O_2 (Chem-Supply, Adelaide, Australia), and 0.2% v/v Triton X-100 (Sigma-Aldrich) in PBS. The sections were incubated overnight with primary antibody

diluted in 2% v/v normal donkey serum and 0.2% v/v Triton X-100 in PBS. The primary antibodies used are EphA2 (1:100; Clone 4B3 provided internally)[42] and anti-myc (1:100; Miltenyl-Biotech). The sections were washed in PBS for 3x20 min before incubating with the secondary antibody. For standard fluorescence immunolabeling, donkey anti-rabbit IgG conjugated to Alexa Fluor 488 (Thermo Fisher Scientific, Melbourne, Australia; Cat# A-21206, RRID:AB_141708) or 555 (Thermo Fisher Scientific; Cat# A-31572, RRID:AB_16254), donkey anti-mouse IgG conjugated to Alexa Fluor 488 (Thermo Fisher Scientific; Cat# A-21202, 555 (1:500; Thermo Fisher Scientific; Cat# A-31570, RRID:AB_2536180) were diluted 1:500 in PBS containing 0.2% v/v Triton X-100 and incubated for 3 hr in a humidified light-protected chamber. For amplification fluorescence immunolabeling, biotinylated donkey anti-rabbit IgG was diluted 1:500 in PBS containing 0.2% v/v Triton X-100 and incubated for 1 hr. The sections were then washed for 3x10 min with PBS before incubation with Streptavidin-Alexa Fluor 647 conjugate (1:500; Thermo Fisher Scientific) diluted in 0.2% Triton X-100 in PBS for 1 hr.

After secondary antibody and amplification incubation, the sections were washed for 3x10 min with PBS and incubated in 4',6-diamidino-2-phenylindole (DAPI) (1: 1000; Thermo Fisher Scientific) in 0.2% Triton X-100 in PBS for 5 min. The sections were then washed for 3x10 min with PBS and coverslipped using ProLong Gold anti-fade reagent (Thermo Fisher Scientific).

Images were acquired using a Diskovery spinning-disk confocal system (Spectral Applied Research Inc, Ontario, CA) built around a Nikon TiE body and equipped with two sCMOS cameras (Andor Zyla 4.2, 2048 x 2048 pixels) and controlled by Nikon NIS software (Nikon, Tokyo, Japan). Images were pseudocolored to permit overlay, cropped, sized, and enhanced for contrast and brightness with Photoshop and Illustrator (Adobe Systems, San Jose, CA) or ImageJ (NIH).

Section 2 – Tumour Staging, Volume Calculations, and Biodistribution

S2.1 – Clinical Equivalent Scans

The current consensus of standard clinical MRI scans for the assessment of brain tumours, as determined by the United States Food and Drug Administration (USFDA) and the National Cancer Institute (NCI), is shown in Table S2.1 for 1.5T and 3T scanners.[1] These scans were assessed for their applicability in mice and were only modified where improved sensitivity or resolution for mice was needed. Any additions or omissions from the prescribed mouse scan protocol were made to focus remaining scan time on the acquisition of dynamic Gadovist® uptake for the purpose of measuring tumour leakiness, as described in Table S2.1.

Table S2.1 - Scans used for glioma diagnosis in mice compared to clinical standards.

Abbreviations: GRE = gradient echo, FLAIR = fluid attenuation inversion recovery, DWI = diffusion weighted image, TSE = turbo spin echo.

MRI Scans		
Contrast[a]	**Human Scan**[37]	**Equivalent Mouse Scan**
Pre	3D T1 GRE	3D T1 GRE (Dixon)
	Axial 2D FLAIR	N/A[b]
	Axial 2D DWI	N/A[c]
	Axial 2D T2 (TSE)	T2-TSE (Sagittal, Coronal, Axial)
Dynamic	N/A	Dynamic GRE – Gadovist®
Post	3D T1 GRE Post-Contrast	3D T1 GRE (Dixon)

	Axial 2D FLAIR	N/A[b]
	Axial 2D DWI	N/A[c]
	Axial 2D T2 (TSE)	T2-TSE (Sagittal, Coronal, Axial)

a – Gadovist®, a clinically standard contrast enhancement agent, was used in mice.
b – FLAIR sequences are known to cause artefacts at 7T and are difficult in smaller subjects
c – DWI in mice currently requires ultra-high fields.[2] A simpler approach to BBB leakiness was used via a dynamic (injected during acquisition) uptake scan.

In the experiments reported in this work, both pre- and post- contrast enhanced 2D & 3D T1 and T2 weighted scans were acquired. In addition to the single axial scan often undertaken in human assessments, coronal and sagittal T2 scans were also taken for better tumour localisation. Fluid attenuation inversion recovery (FLAIR) sequences are recommended for the assessment of cerebrospinal fluid to monitor the presence of vasogenic edema and the effects of radiation therapy, and hence are not useful for analysis of BBB penetration. Similarly, diffusion-weighted imaging (DWI) MRI sequences are used to identify areas of high cellular density for the purpose of measuring treatment response. As neither a full-scale diagnosis nor response to treatment was assessed in this study, a dynamic contrast enhanced T1-weighted image using a gradient echo (GRE) sequence was acquired instead to measure the degree of leakiness of the tumour vasculature.

S2.2 – Volume Calculations and Custom Staging

Averages of the minimum, maximum, and median values of the longest tumour diameters across all mice with tumours greater than the minimum threshold were calculated and 4 stages were developed from these ranges. The longest diameter of the tumour was measured for each plane from the T2 weighted images (600 µm slice thickness), the volume calculated using the general formula for an ellipsoid and plotted by stage in Figure 2B in the main text. The full calculations for these stages and tumour progression information can be found in Section S2.3 of this supplementary information and are also highlighted in Figure 2B in the main text. The height of each bar represents the average value for the tumour volume at each stage, with each point the actual recorded value for each mouse measured at that stage. Not all mice survived to late stage, so the data represents the total aggregated measurements of all mice with tumours across multiple scan times (n = 13 mice, 27 assessment points). The absolute median value of all maximum tumour diameters was calculated (~3.76 mm) and together with the minimum (0.7 mm) and maximum (6.00 mm) values for tumour diameters measured a stratified scale relating tumour volume (by longest diameter) as a measure of tumour progression was prepared (Figure 2B in the main text). Each group was tested for statistical significance to ensure a fair-weighted distribution, and the means of all groups were found to be statistically different from each other (See main text, Figure 2B).

The equivalent limits for mouse brain tumours were based on RECIST values using Equation S2.1, and shown in Table S2.2 below.[3] Finally, the volumes of each tumour was calculated using Equation S2.2, where r_{cor}, r_{ax}, and r_{sag} are the radius for the longest diameter for the coronal, axial, and sagittal planes, respectively (Table S2.3).

Table S2.2 – Human and mouse brain and tumour comparison

Subject	Average Brain Width [mm]	Minimal Tumour Width [mm]
Human	140[2]	10
Mouse	10	0.7

Equation S2.1 – Calculation of RECIST equivalent of minimal mouse brain tumour

$$TumourDiameter_{Mouse} = \left(\frac{BrainDiameter_{Mouse}}{BrainDiameter_{Human}}\right) \times TumourDiameter_{Human}$$

Table S2.3 – Table of longest diameters and volumes for each mouse

Mouse ID	Days Post-Tamoxifen	Longest Diameter			Tumour Volume [mm^3]
		Coronal	*Axial*	*Sagittal*	
F195	93	2.47	2.05	2.27	6.02
F195	97	3.76	3.46	3.36	22.89
F195	107	3.91	3.58	3.53	25.87
F195	125	3.92	3.27	2.94	19.73
F244	114	3.59	3.15	3.29	19.48
F244	122	3.93	3.29	4.73	32.02
F245	105	2.14	2.85	4.46	14.24
F245	114	3.27	4.11	5.54	38.99
F245	122	5.65	6.00	5.54	98.33
F248	122	2.13	2.37	1.76	4.65
F249	90	3.37	3.09	3.49	19.03
F250	90	2.51	1.38	3.08	5.59
F250	97	4.05	1.44	3.28	10.02
F250	109	4.30	1.43	3.48	11.20
F250	118	5.28	2.11	3.69	21.52
F251	90	2.74	2.36	3.42	11.58
F251	97	2.98	2.53	3.65	14.41
F251	109	4.74	2.90	5.14	36.99
F251	118	5.69	3.75	5.41	60.44
F252	90	3.04	2.13	2.00	6.78
F252	97	3.97	3.27	3.32	22.57
F293*	81	4.00	3.29	5.00	34.45
F293**	81	2.34	1.28	3.26	5.11
F294	81	0.84	0.86	0.98	0.37
F296	81	2.08	1.73	1.78	3.35
F296	83	2.67	2.82	2.17	8.55
F297	81	4.09	4.14	3.80	33.69
M342	200	0.96	0.90	0.82	0.37
M342	203	1.13	0.86	1.19	0.61

Note: F293 had 2 tumours: Frontal, and Parietal**. Mouse IDs were assigned using an in-house numbering system, where each number denotes a unique mouse across one or more timepoints. Days post-tamoxifen refer to the number of days after tamoxifen was injected to induce the genetic knockouts. Some mice were measured at multiple timepoints for this reason and therefore have repeated values in this table.*

Table S2.4 – Table of upper and lower bounds for staging categories

Category	Lower Bound [mm]	Upper Bound [mm]
Unmeasurable	0.0	0.7
Early	0.7	2.5
Middle	2.5	4.5
Late	4.5	∞

Equation S2.2 – Calculation of tumour volume

$$V_{Tumour} = \left(\frac{4}{3}\pi\right) r_{cor} r_{ax} r_{sag}$$

S2.4 – Biodistribution

Following image acquisition at 36 hours post injection, animals were euthanised by cervical dislocation. Blood was sampled and tissues collected and cleaned of excess blood and weighed for *ex vivo* analysis. A Perkin PerkinElmer 2480 Automatic Gamma Counter was used to measure radioactivity in tissues. The gamma counter was calibrated using known samples of ^{64}Cu and measured activity presented as %ID/g based on injected activities. Figure S2.4.1 shows the *ex vivo* biodistribution of all nanoparticles at 36 hours post injection. As several mice were not able to be assessed for biodistribution in the bNP-EphA2, bNP, and sNP groups, comparison data in previously published MDA-MB-468 breast cancer xenograft model[4] are shown in Figure S2.4.2.

Figure S2.4.1 – *Ex vivo* biodistribution in GBM Mice

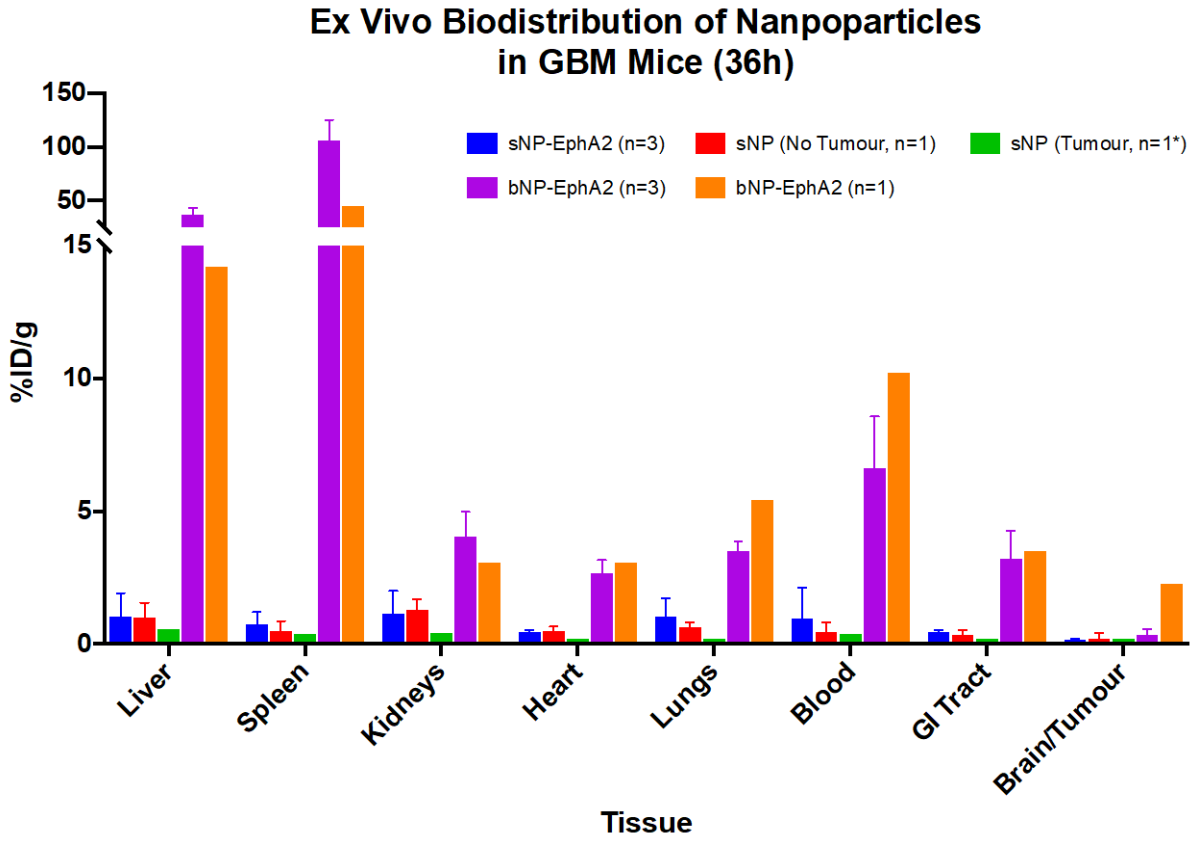

Figure S2.4.2 – *Ex vivo* Biodistribution in MDA-MB-468 Mice.

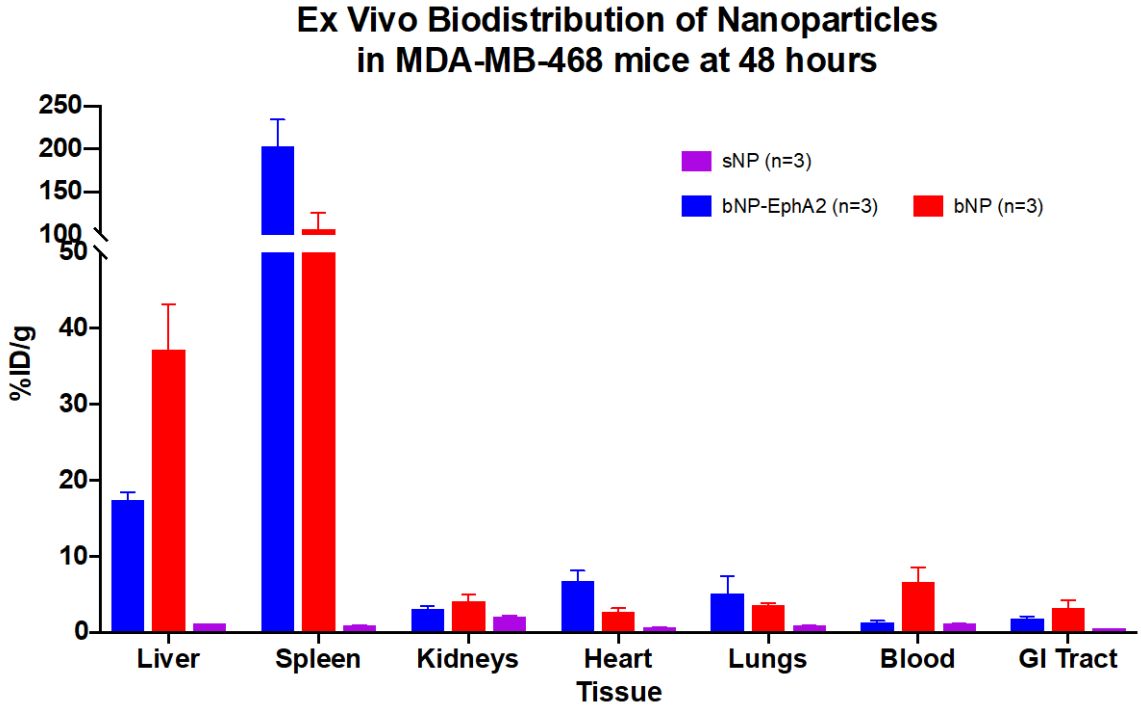

Section 3 – Tumour Leakiness Calculations

The degree of tumour associated vasculature leakiness was estimated by measuring the relative rate of Gadovist® uptake in the tumour using a dynamically acquired T1-weighted MRI image. Because a higher degree of leakiness is an indication of the extent of the gaps formed in the tight junctions, this should directly correlate with the access to the tumour tissue through the BBB by larger nanomedicines. Therefore, it is hypothesised that a higher degree of leakiness will result in a high degree of permeation and retention into brain tumours. In a healthy brain Gadovist® will not permeate across the BBB (Figure 1A in the main text). Upon the internal pressure exerted on the BBB by a growing tumour mass and more rapid development of the surrounding vasculature, the integrity of the BBB weakens and Gadovist® can permeate into the highly vascularized tumour tissue. Because Gadovist® can define the point at which the tumour BBB was leaky independently from the tumour volume, it was used to monitor the degree of leakiness of the BBB. The rate of accumulation of the Gadovist® in the tumour was assessed by drawing a region of interest (ROI) around the tumour in the T1-weighted dynamic MRI scan and measuring the change in signal intensity over time.

The accumulation of Gadovist® in the tumour was monitored over a 10-minute dynamic scan (1 image at each slice [5x1mm], every 3 seconds) to assess the leakiness of the BBB. The time acquired data for the dynamic Gadovist® uptake was opened in Osirix MD (v 9.0.1) using the 4D visualization mode. A 2D circular region of interest (ROI) was drawn around the tumour in the slice of best view, and the mean intensity over time was exported as a CSV using the ROI Enhancement Plugin as a tumour uptake curve for each mouse at each assessable time point. Plots were normalized to overcome susceptibility artefacts from the MRI by dividing all mean intensity values by the minimum value from each dataset. Starting times were all set as 0 for when the curve began to rise, and the full scan time (~9.55-10 min) was plotted (Figure S3.1). After approximately the first 3-4 minutes a slow and gradual incline was noticed, indicating a

change in the kinetics of Gadovist® uptake, which can partially be attributed to T2* effects as mentioned in the main text. Therefore, the first 200 seconds of data were used to analyse the initial uptake only of the Gadovist® (Figure S3.2), as this initial timeframe represents only a leakiness in the tumour vasculature. The area under the curve for each uptake plot was measured using the built-in "XY analyses – Area under curve" tool in GraphPad Prism (v 7.0c) with the data output shown in Table S3.1. The area under the curve was measured using the trapezoid rule shown in Equation S3.1, whereby Y1 and Y2 are the height of the curve at point 1 and 2 along the curve (mean intensity values), and ΔX is the width between Y1 and Y2 (change in time).

Finally, where values existed for both a tumour volume and leakiness across all mice at all timepoints, they were correlated to each other to see if there was any direct comparison that could be made between the values. As the plot in Figure S3.3 shows, no direct correlation could be made, and hence separate staging was needed.

Equation S3.1 – Calculation of Initial Area Under Curve (IAUC)

$$IAUC = \Delta X \left(\frac{Y1 + Y2}{2} \right)$$

Figure S3.1 – Normalised Gadovist® intensity plots for full scan time (~600 sec)

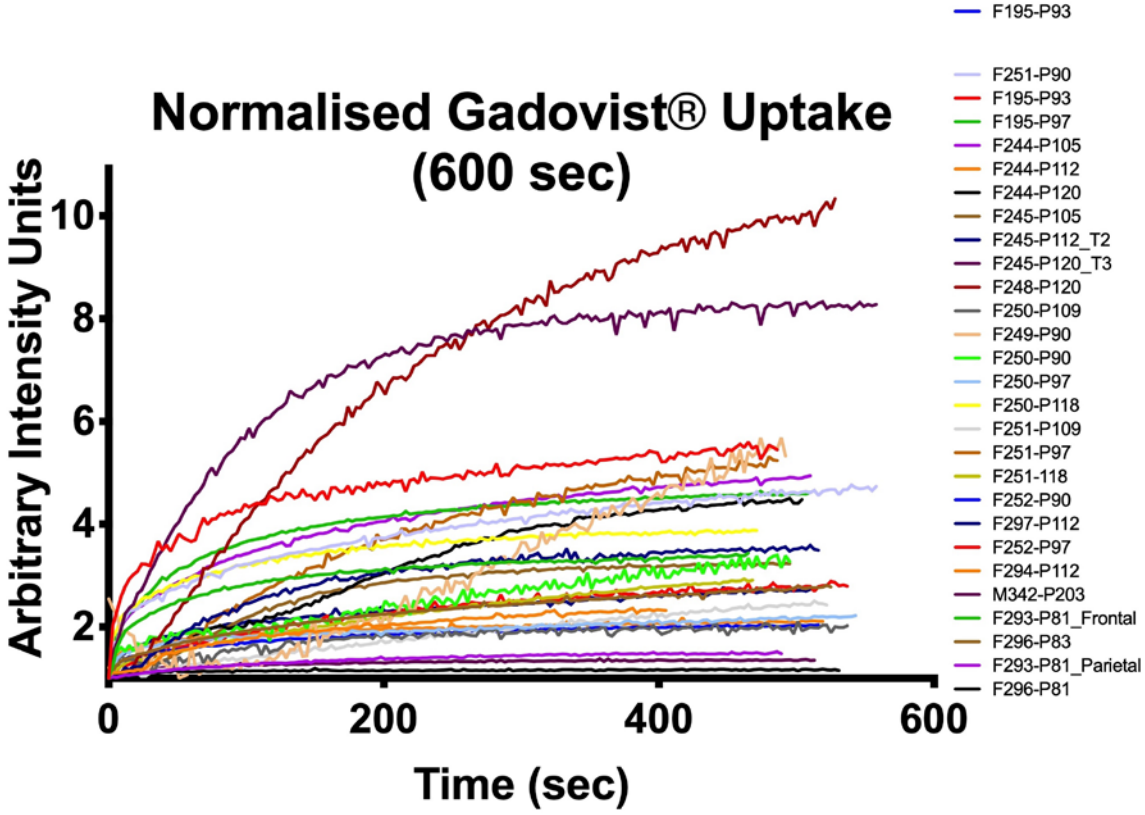

Figure S3.2 – Normalised Gadovist® intensity plots for first 200 seconds

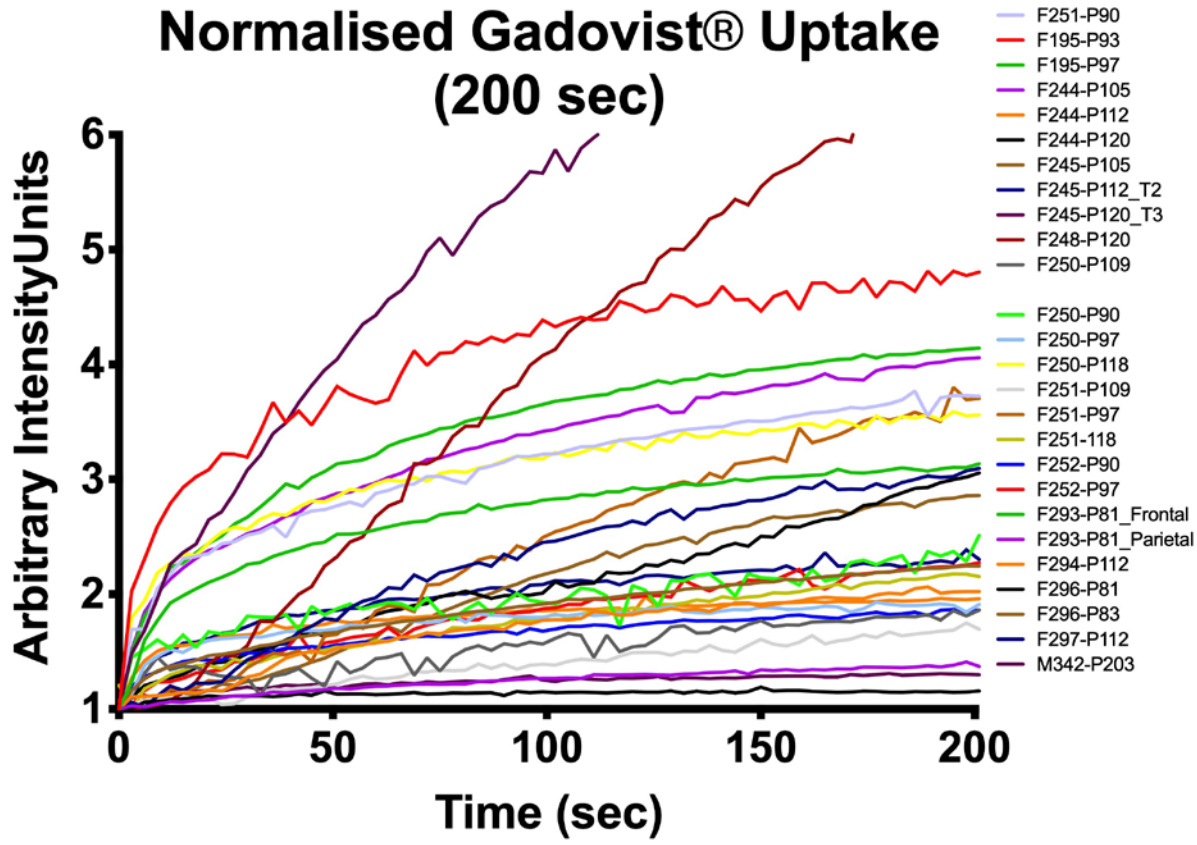

Table S3.1 – Area under the curve analysis data from plots in Figure S3.1

Mouse ID – Post Tamoxifen Date	First X	Last X	Peak X	Peak Y	Area	%Area	Total Area	Total Peak Area
F195-P93	0	201	189	4.8	817	100	817	817
F195-P97	0	201	201	3.1	539	100	539	539
F244-P105	0	201	198	1.4	250	100	250	250
F244-P112	0	201	189	2.1	339	100	339	339
F244-P120	0	201	150	1.2	228	100	228	228
F245-P105	0	201	198	2.2	375	100	375	375
F245-P112	0	201	201	3.1	459	100	459	459
F245-P120	0	201	201	7.3	1056	100	1056	1056
F248-P120	0	201	195	6.8	791	100	791	791
F249-P90	0	201	0	2.5	318	100	318	318
F250-P90	0	201	201	2.5	394	100	394	394
F250-P97	0	201	177	1.9	355	100	355	355
F250-P109	0	201	201	1.9	310	100	310	310
F250-P118	0	201	195	3.6	618	100	618	618
F251-P90	0	201	186	3.8	620	100	620	620
F251-P97	0	201	195	3.8	488	100	488	488
F251-P109	0	201	198	1.7	279	100	279	279
F251-118	0	201	195	2.2	353	100	353	353
F252-P90	0	201	195	1.9	333	100	333	333
F252-P97	0	201	201	2.3	366	100	366	366
F293-P81*	0	201	201	4.1	691	100	691	691
F293-P81**	0	201	201	4.1	656	100	656	656
F294-P112	0	201	123	2	363	100	363	363
F296-P81	0	201	201	3.1	421	100	421	421
F296-P83	0	201	201	2.9	414	100	414	414
F297-P112	0	201	198	2.4	402	100	402	402
M342-P203	0	201	180	1.3	249	100	249	249

Note: Baseline and number of peaks for all area's measured were 0 and 1, respectively. F293 had 2 tumours: Frontal, and Parietal**. The P-notation in the Mouse ID column refers to days post-tamoxifen, and is in reference to the number of days after tamoxifen was injected to induce the genetic knockouts. Some mice were measured at multiple timepoints for this reason and therefore have repeated values in this table.*

Figure S3.3 – Correlation of staging by volume and leakiness

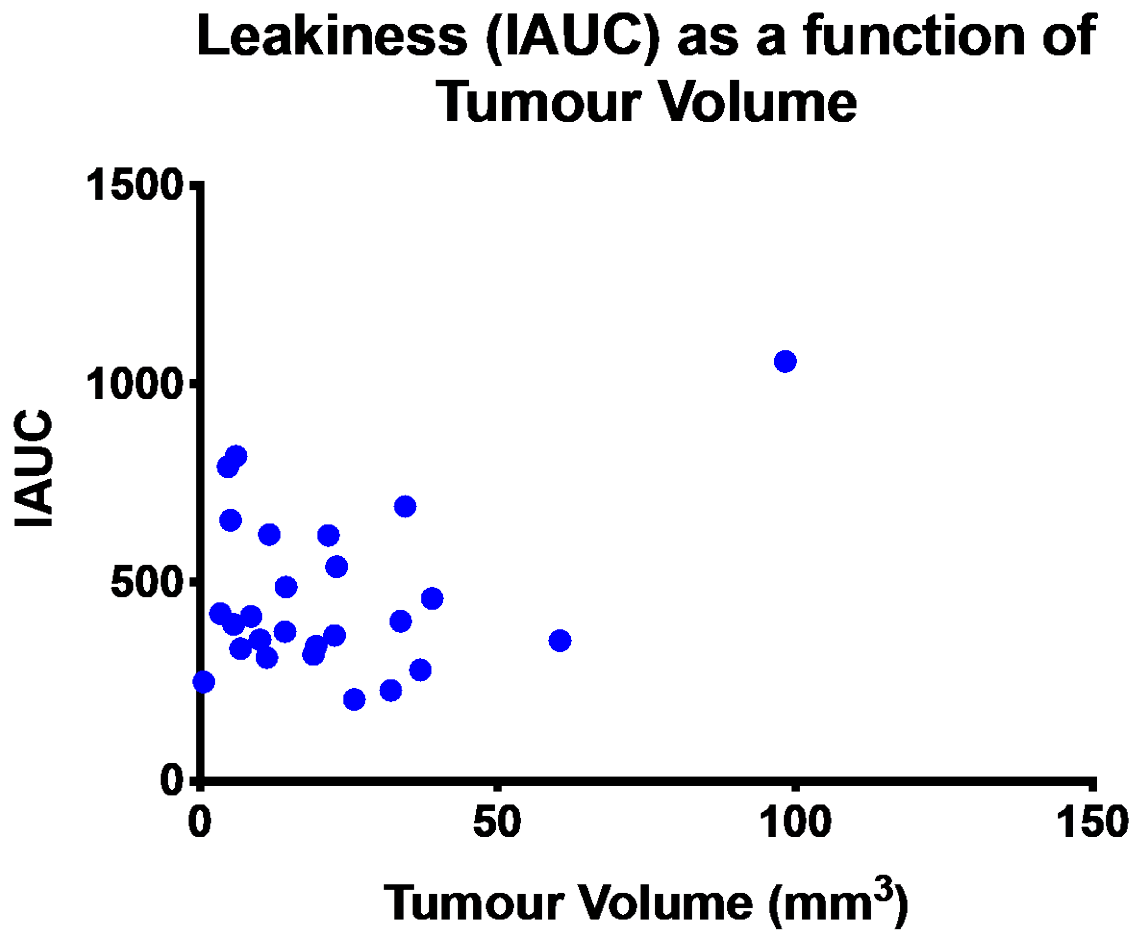

Section 4 – Tumour size progression (RECIST)

For any mice that were able to be assessed for 3 or more consecutive time points, tumour progression and growth were monitored by measuring the longest tumour diameter using the line ROI tool in Osirix MD (v 9.01) in each plane (coronal, axial, or sagittal). The longest diameter overall was used to track the change, as per RECIST criteria, is shown in Figure S4.1

Figure S4.1 – Longitudinal assessment of tumour progression

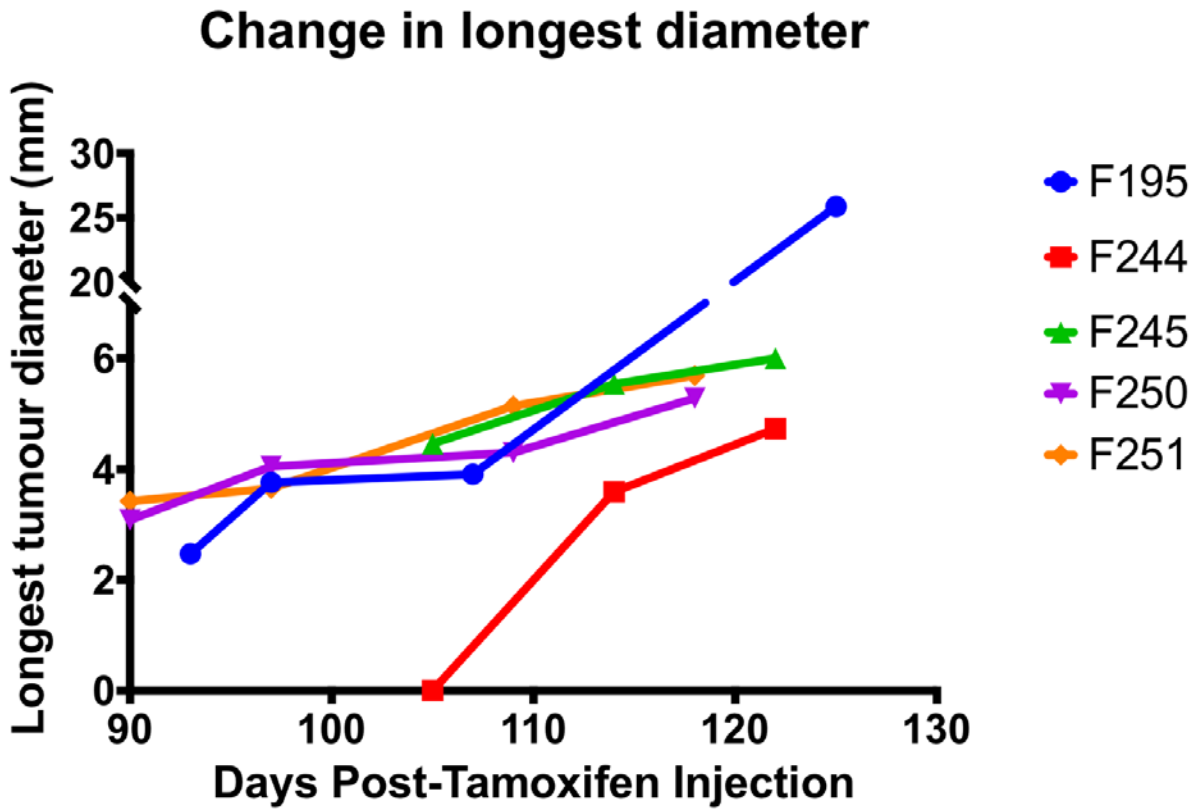

Section 5 – Distribution of tumour location

Figure S5.1 – Image map of tumour locations

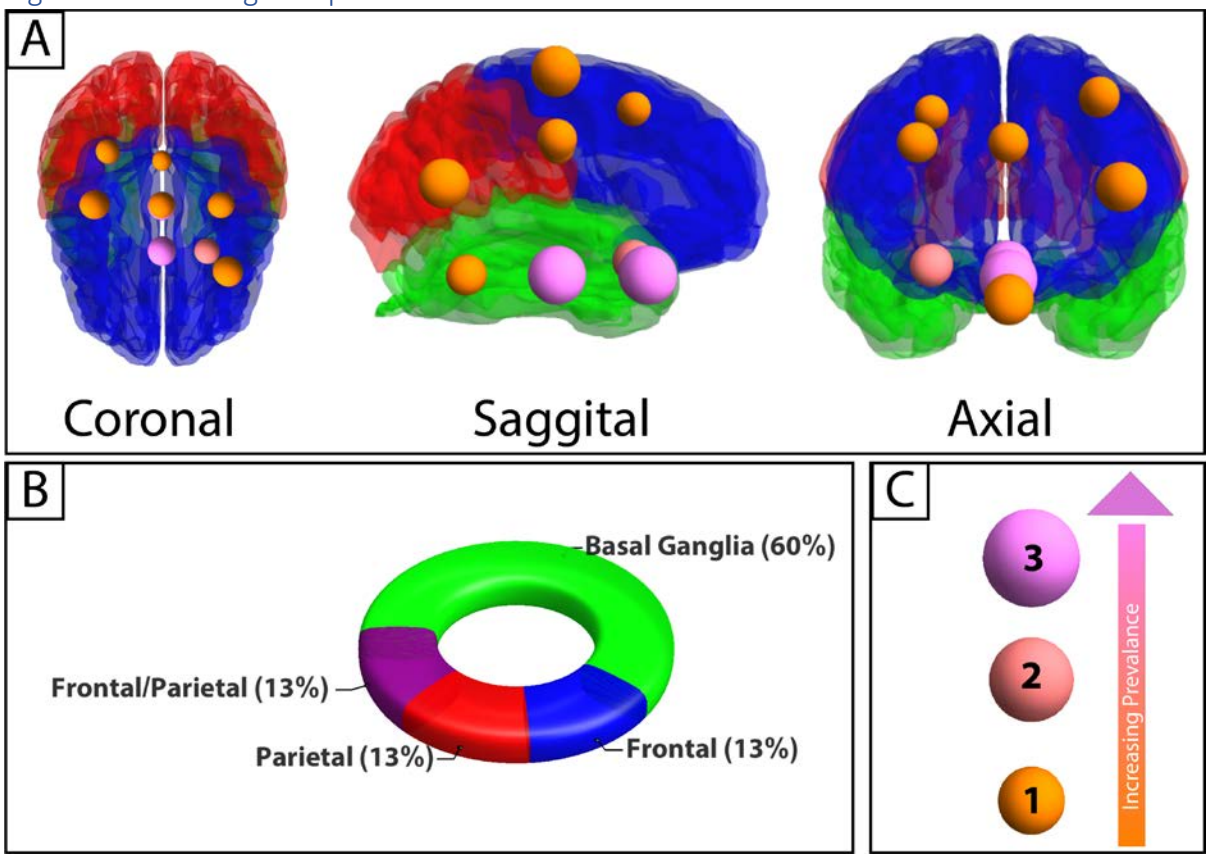

A) Pictorial representation of the various locations of spontaneous tumour growth, and B) their distribution graphically is shown with colour codes of red, blue, and green for Frontal, Parietal, and Basal Ganglia lobes, respectively. C) Both the colour and size of the spheres indicate the prevalence of tumours at that approximate location. Data from all mice in the study that grew tumours to a measurable size (n = 14).

The rate of tumour growth was found to be dictated significantly by the location of the tumour. In general, areas of high vascularization such as the Basal Ganglia and tissue surrounding major arterial pathways such as the Circle of Willis grow larger tumours and in higher degrees of prevalence. This is likely due to higher nutrient availability and blood supply from a more accessible native arterial supply. Nonetheless, it has a significant impact on the distribution of tumours and their average growth and progression throughout the study. The approximate location of each tumour measured in the previous section (n=13 mice, 27 assessment points) is plotted in Figure S5.1. When measuring each tumour at each assessment point in the MRI, the anatomical positioning of that tumour was recorded with respect to lobe (Frontal, Parietal, Basal Ganglia, etc.), axial (left, right medial), and sagittal (dorsal, ventral, medial) locations. These locale were then converted into x,y,z coordinates. The diameter and colour of the sphere are representative of the number of occurrences in that particular location. For full details of how these points were plotted, the reader is directed to the supplementary information (Supplementary, Section 5). Overall a wide distribution of locations for tumour formation were observed, highlighting the spontaneity of the model and showing the utility of this methodology for analysis of tumour progression. More importantly, the trends observed in Figure 2 in the main text are representative of a wide variety of tumour sizes and locale.

As described above, the location of each tumour was given a coordinate system in the 3D space of the brain by plane as shown in Figure S5.2. Tumour locations were first defined by the lobe in which the tumour was found followed by right, medial, or left of the central axis for both the coronal and sagittal planes. All tumours were found in either the frontal lobe, parietal lobe, or the Basal Ganglia (highlighted in the main text Figure 3a). Tumour locations in the X (coronal) and Y (sagittal) plane were designated by Left/Right and Dorsal/Ventral (near spine/near abdomen), respectively. Each tumour location was given a coordinate number as per the rules in Table S5.1, and the number of times a tumour appeared in this location was counted (Table S5.2). This 4-point system (x, y, z, prevalence) was then used to plot in a 3D bubble chart using Mathematica (v 11.1.0.0) and overlaid on a schematic representation of the brain in each major plane using the built in AnatomyPlot3D functionality to show the data in Figure 3 from the main text.

Figure S5.2 – Location of planes and coordinates used for defining tumour location

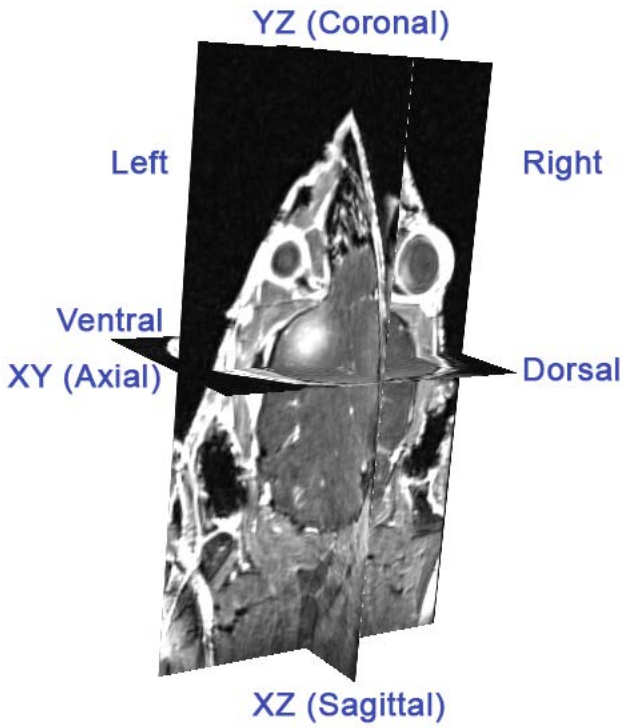

Table S5.1 – Coordinate system used to define tumour location

Plane	Position	Coordinate
Coronal (YZ)	Left	-1
	Medial	0
	Right	1
Sagittal (XZ)	Dorsal	-1
	Medial	0
	Ventral	1
Axial (XY)	Frontal Lobe	3
	Frontal/Parietal Lobe	2.5
	Parietal Lobe	2
	Basal Ganglia	1

Table S5.2 – Summary of tumour location data used to make Figure S5.1

Corresponding Mouse ID(s)	Coronal (YZ)	Sagittal (XZ)	Axial (XY)	Prevalence	Plotted Coordinate
F195	-1	1	3	1	(-1,1,3,1)
F244, F245, F296	0	0	1	3	(0,0,1,3)
F248, F249, F295	0	1	1	3	(0,1,1,3)
F250, F251	-1	1	1	2	(-1,1,1,2)
F252	1	-1	2	1	(1,-1,2,1)
F293	1	0	3	1	(1,0,3,1)
F293	0	0	3	1	(0,0,3,1)
F294	-1	0	2.5	1	(-1,0,2.5,1)
F297	0	0	2.5	1	(0,0,2.5,1)
M342	0	-1	1	1	(0,-1,1,1)

Section 6 – Quantifying small and big NP uptake in the tumour

Both targeted and untargeted small (sNP) and large (bNP) nanoparticles were injected at various stages of tumour progression in healthy and tumour-bearing mice (n=16 mice, 20 assessment points). The ^{64}Cu-polymer was allowed to circulate for 36 h and the accumulation was quantified as percent injected dose per gram (%ID/g) in the tumour with PET, and simultaneously anatomically registered with high precision using MRI (early and late stage representative image shown in Figure 3A in the main text). Gadovist® was co-injected to obtain the scans necessary for the determination of volume and leakiness as described above. Of all the mice scanned, 8 (sNP-EphA2: n=3, bNP-EphA2: n=3, sNP no targeting: n=1, bNP no targeting: n=1) developed a stage of tumour where the nanoparticles were able to cross the BBB (%ID/g of tumour > brain & background) and accumulate in the tumour.

Three-dimensional ROIs of the tumour leaky tumour tissue were created by using the subtraction T1-weighted images before and after Gadovist® administration (post minus pre) and using thresholding to isolate the regions of high Gadovist® uptake. Both the PET and MRI data were registered to each other and the ROI created from the MRI image was applied to the PET image. The percent injected dose per gram (%ID/g) was calculated from the volume

by the general formula in Equation S6.1, assuming a density of 1 g/mL for all tissue. All ROI measurements and calculations for this data were done using Inveon Research Workplace (v 4.2) software by Siemens Molecular Imaging. The values for all mice injected with either sNP, sNP-EphA2, bNP, or bNP-EphA2 are summarized in Table S6.1. In each case, if the %ID/g of either the background (outside the mouse) or the healthy brain tissue were greater than what was measured for the tumour, it was assumed to have no nanoparticle pass and was given a null value for %ID/g. The data below was combined with tumour volume and leakiness data to create Figure 5C in the main text. Also shown is the radioisotopic TLC to validate the ^{64}Cu labelling step in Figure S6.1 as discussed in the main text.

The dependence nanoparticle accumulation by tumour location was also assessed by plotting the uptake of the nanoparticles for each major tumour location defined as a function BBB leakiness (Figure S6.2 & S6.3). As the location of the tumour also highly influenced the degree of leakiness, the plots show the crossing staged by leakiness by general location of the tumour at either the frontal/parietal lobes or at the basal ganglia. Any point on the baseline indicates where a NP was tested but was not able to cross the BBB and accumulate in the tumour.

Equation S6.1 – Percent Injected Dose per gram

$$\%ID/g = \frac{\left(\frac{Dose_{Tumour}}{Dose_{Injected}} \times 100\%\right)}{Volume_{Tumour\_ROI} \times density_{Tumour}}$$

Table S6.1 – Summary of %ID/g for all mice injected with sNP or bNP

Mouse ID	Stage by Tumour Volume	Stage by Tumour Leakiness	Compound Injected	%ID/g
F195	Mid	Early	sNP-EphA2	0.12
F198	Healthy	Early	sNP-EphA2	0.00
F244	Late	Early	sNP-EphA2	0.30
F245	Late	Late	sNP-EphA2	0.14
F248	Early	Late	sNP-EphA2	0.00
F250	Late	Late	bNP-EphA2	0.98
F251	Late	Mid	bNP-EphA2	0.78
F253	Healthy	Healthy	bNP-EphA2	0.00
F293	Healthy	Healthy	sNP-EphA2	0.00
F294	Healthy	Healthy	bNP-EphA2	0.00
F295	Healthy	Healthy	bNP-EphA2	0.00
F296	Mid	Late	bNP-EphA2	3.90
F297	Healthy	Healthy	bNP	0.00
F298	Healthy	Healthy	sNP	0.00
F294	Early	Healthy	bNP-EphA2	0.00
F295	Healthy	Healthy	bNP-EphA2	0.00
F297	Mid	Late	bNP	0.80
F361	Healthy	Healthy	sNP	0.00
M342	Early	Mid	sNP	0.46

Figure S6.1 – Example Radio TLC validating labelling procedure with free and unbound ^{64}Cu.

A representative TLC of the sNP before BsAb conjugation is shown below. No free ^{64}Cu was seen and the radiopurity was calculated to be 100%. The same radiopurity was obtained for all samples prior to BsAb conjugation and injection.

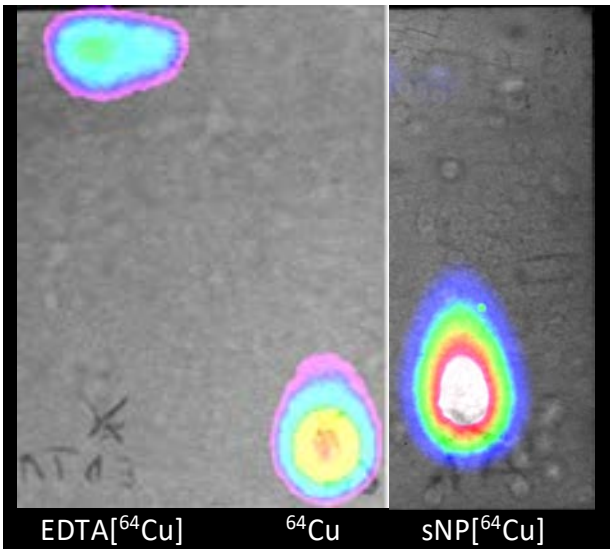

Figure S6.2 – Accumulation of NPs in the Frontal/Parietal Lobes staged by Leakiness

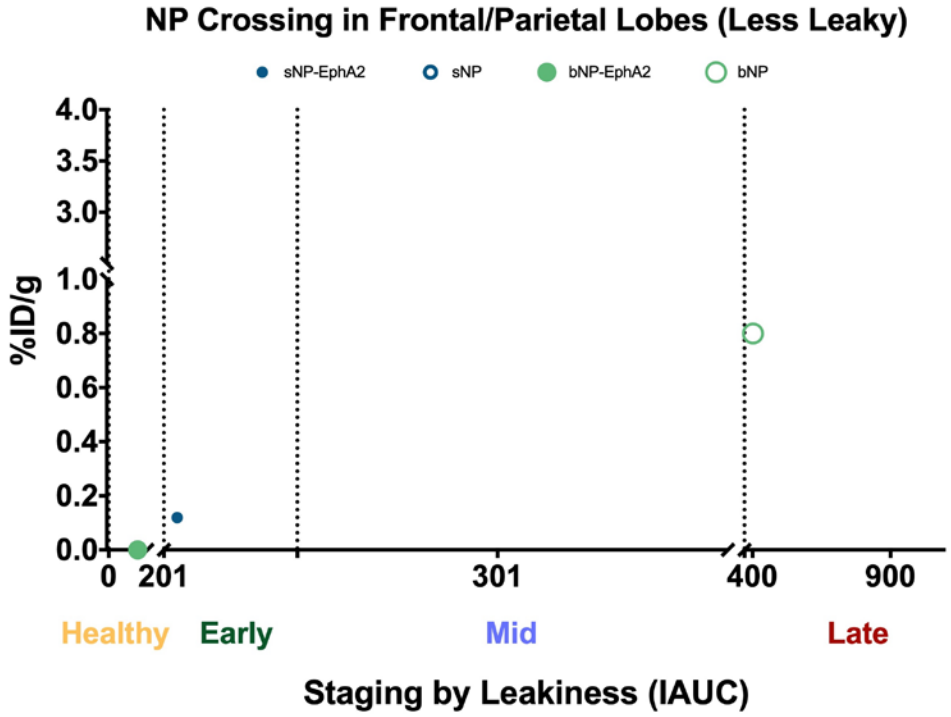

Figure S6.3 – Accumulation of NPs in the Basal Ganglia staged by Leakiness

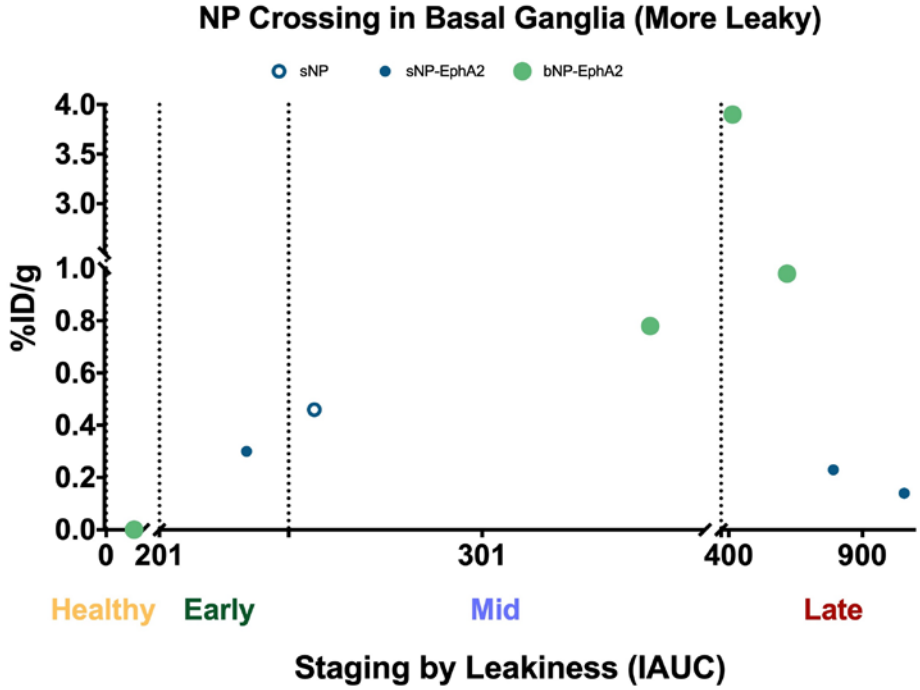

Section 7 – Validation of EphA2 Expression

In addition to the confocal microscopy shown in Figure 6 in the main text, further tissue samples were assessed and are shown in Figure S7.1. As a human antibody was used in this experiment, the sequence was checked for homology against mouse EphA2, the results of which are shown in Figure S7.2. To validate this binding, the affinity for the 4B3 variant of the EphA2 antibody against murine EphA2 receptors was validated with an ELISA (Figure S7.3).

Figure S7.1 – All confocal microscopy

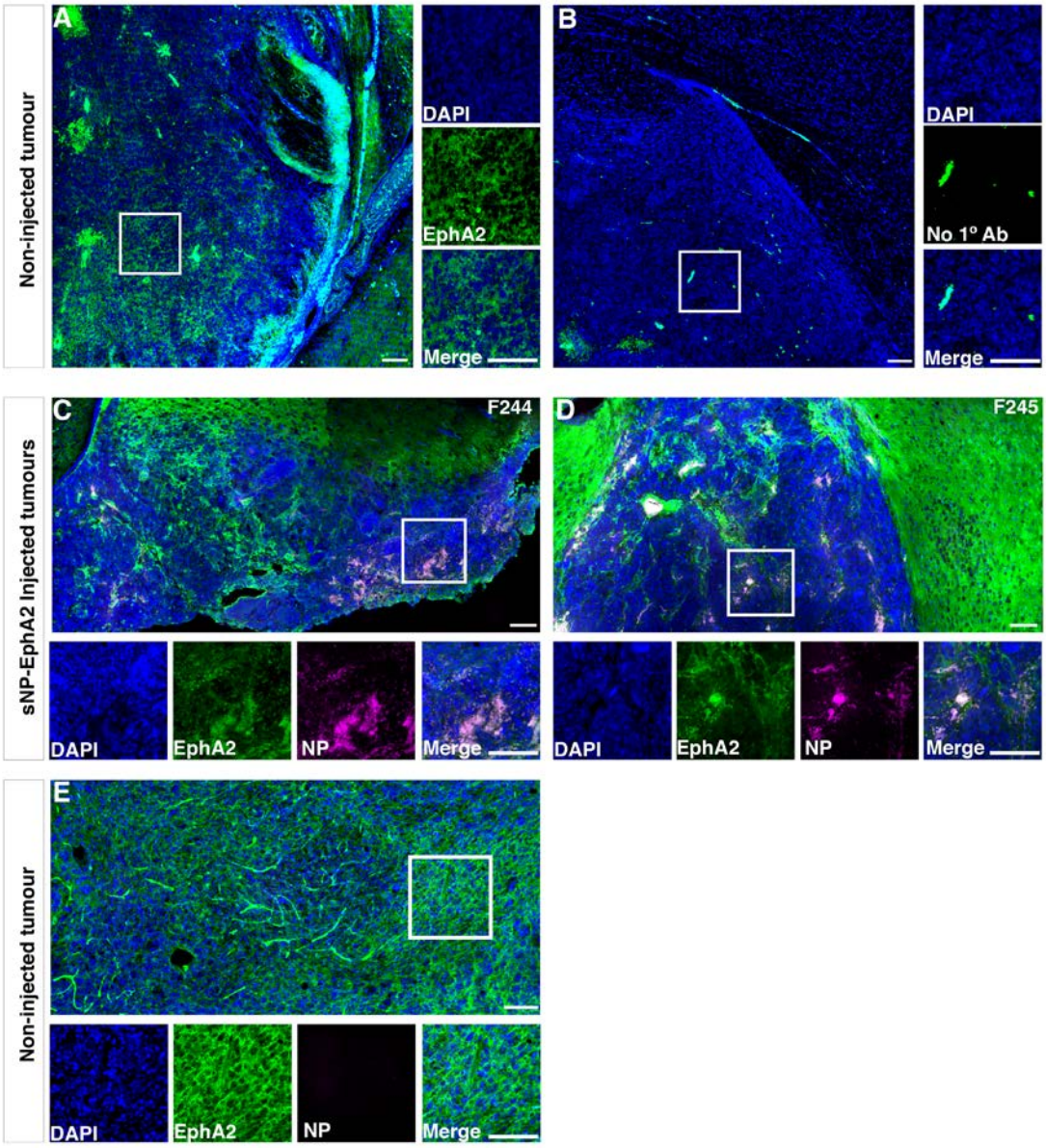

Confocal microscopy of brain tumours from mice with a small nanoparticle (sNP-EphA2) injected and without nanoparticle injected. (A) Expression of EphA2 (green) was observed in brain tumour without nanoparticle injection. (B) No specific EphA2 signal (green) was observed in the same tumour tissue as in A if no primary antibody was incubated, confirming the specificity of EphA2 primary antibody. (C,D) Co-localization of EphA2 (green) and Cy5 dye-incorporated nanoparticle (magenta) was observed in tumour tissues from nanoparticle injected mice. (E) No signal of Cy5 dye was observed in tumour tissues from non-injected mouse. For all images, DAPI staining (blue) is for the nucleus. Scale bars = 50mm.

Figure S7.2 – Homology Analysis of 4B3 Antibody

The amino acid sequences of human and mouse EphA2 proteins were derived from the uniprot online database (https://www.uniprot.org/).The sequences were aligned using ClustalW to estimate homology and the potential cross-reactivity of the 4B3 MAb (anti-human EphA2) with mouse EphA2. The sequences were highly homologous with >90% homology between species. The sequence for the mouse alternative of EphA2 is **in bold font** in the first line of the output below.

```
CLUSTAL 2.1 multiple sequence alignment


M_EphA2_Q03145      ---KEVVLLDFAAMKGELGWLTHPYGKGWDLMQNIMDDMPIYMYSVCNVVSGDQDNWLRT
h_EphA2_P29317      AQGKEVVLLDFAAAGGELGWLTHPYGKGWDLMQNIMNDMPIYMYSVCNVMSGDQDNWLRT
                       **********  **********************:************:**********

M_EphA2_Q03145      NWVYREEAERIFIELKFTVRDCNSFPGGASSCKETFNLYYAESDVDYGTNFQKRQFTKID
h_EphA2_P29317      NWVYRGEAERIFIELKFTVRDCNSFPGGASSCKETFNLYYAESDLDYGTNFQKRLFTKID
                    ***** ************************************:********* *****

M_EphA2_Q03145      TIAPDEITVSSDFEARNVKLNVEERMVGPLTRKGFYLAFQDIGACVALLSVRVYYKKCPE
h_EphA2_P29317      TIAPDEITVSSDFEARHVKLNVEERSVGPLTRKGFYLAFQDIGACVALLSVRVYYKKCPE
                    ****************:******** **********************************

M_EphA2_Q03145      MLQSLARFPETIAVAVSDTQPLATVAGTCVDHAVVPYGGEGPLMHCTVDGEWLVPIGQCL
h_EphA2_P29317      LLQGLAHFPETIAG--SDAPSLATVAGTCVDHAVVPPGGEEPRMHCAVDGEWLVPIGQCL
                    :**.**:******   **: .*************** *** * ***:**************

M_EphA2_Q03145      CQEGYEKVEDACRACSPGFFKSEASESPCLECPEHTLPSTEGATSCQCEEGYFRAPEDPL
h_EphA2_P29317      CQAGYEKVEDACQACSPGFFKFEASESPCLECPEHTLPSPEGATSCECEEGFFRAPQDPA
                    ** *********:******** *****************.******:****:****:**

M_EphA2_Q03145      SMSCTRPPSAPNYLTAIGMGAKVELRWTAPKDTGGRQDIVYSVTCEQCWPESGECGPCEA
h_EphA2_P29317      SMPCTRPPSAPHYLTAVGMGAKVELRWTPPQDSGGREDIVYSVTCEQCWPESGECGPCEA
                    **.********:****:***********.*:*:***:**********************

M_EphA2_Q03145      SVRYSEPPHALTRTSVTVSDLEPHMNYTFAVEARNGVSGLVTSRSFRTASVSINQTEPPK
h_EphA2_P29317      SVRYSEPPHGLTRTSVTVSDLEPHMNYTFTVEARNGVSGLVTSRSFRTASVSINQTEPPK
                    *********.******************:******************************

M_EphA2_Q03145      VRLEDRSTTSLSVTWSIPVSQQSRVWKYEVTYRKKGDANSYNVRRTEGFSVTLDDLAPDT
h_EphA2_P29317      VRLEGRSTTSLSVSWSIPPPQQSRVWKYEVTYRKKGDSNSYNVRRTEGFSVTLDDLAPDT
                    ****.********:**** .*****************:**********************

M_EphA2_Q03145      TYLVQVQALTQEGQGAGSKVHEFQTLSTEGSANMAVIGGVAVGVVLLLVLAGVGLFIHRR
h_EphA2_P29317      TYLVQVQALTQEGQGAGSKVHEFQTLSPEGSGNLAVIGGVAVGVVLLLVLAGVGFFIHRR
                    ****************************.***.*:********************:*****

M_EphA2_Q03145      RRNLRARQSSEDVRFSKSEQLKPLKTYVDPHTYEDPNQAVLKFTTEIHPSCVARQKVIGA
h_EphA2_P29317      RKNQRARQSPEDVYFSKSEQLKPLKTYVDPHTYEDPNQAVLKFTTEIHPSCVTRQKVIGA
                    *:* *****.*** ************************************:*******

M_EphA2_Q03145      GEFGEVYKGTLKASSGKKEIPVAIKTLKAGYTEKQRVDFLSEASIMGQFSHHNIIRLEGV
h_EphA2_P29317      GEFGEVYKGMLKTSSGKKEVPVAIKTLKAGYTEKQRVDFLGEAGIMGQFSHHNIIRLEGV
                    ********* **:******:********************.**.***************

M_EphA2_Q03145      VSKYKPMMIITEYMENGALDKFLREKDGEFSVLQLVGMLRGIASGMKYLANMNYVHRDLA
h_EphA2_P29317      ISKYKPMMIITEYMENGALDKFLREKDGEFSVLQLVGMLRGIAAGMKYLANMNYVHRDLA
                    :*****************************************:****************

M_EphA2_Q03145      ARNILVNSNLVCKVSDFGLSRVLEDDPEATYTTSGGKIPIRWTAPEAISYRKFTSASDVW
h_EphA2_P29317      ARNILVNSNLVCKVSDFGLSRVLEDDPEATYTTSGGKIPIRWTAPEAISYRKFTSASDVW
                    ************************************************************

M_EphA2_Q03145      SYGIVMWEVMTYGERPYWELSNHEVMKAINDGFRLPTPMDCPSAIYQLMMQCWQQERSRR
h_EphA2_P29317      SFGIVMWEVMTYGERPYWELSNHEVMKAINDGFRLPTPMDCPSAIYQLMMQCWQQERARR
                    *:************************************************:**

M_EphA2_Q03145      PKFADIVSILDKLIRAPDSLKTLADFDPRVSIRLPSTSGSEGVPFRTVSEWLESIKMQQY
h_EphA2_P29317      PKFADIVSILDKLIRAPDSLKTLADFDPRVSIRLPSTSGSEGVPFRTVSEWLESIKMQQY
                    ************************************************************

M_EphA2_Q03145      TEHFMVAGYTAIEKVVQMSNEDIKRIGVRLPGHQKRIAYSLLGLKDQVNTVGIPI
h_EphA2_P29317      TEHFMAAGYTAIEKVVQMTNDDIKRIGVRLPGHQKRIAYSLLGLKDQVNTVGIPI
                    *****.************:*:**********************************
```

Figure S7.3 – ELISA of 4B3 Antibody

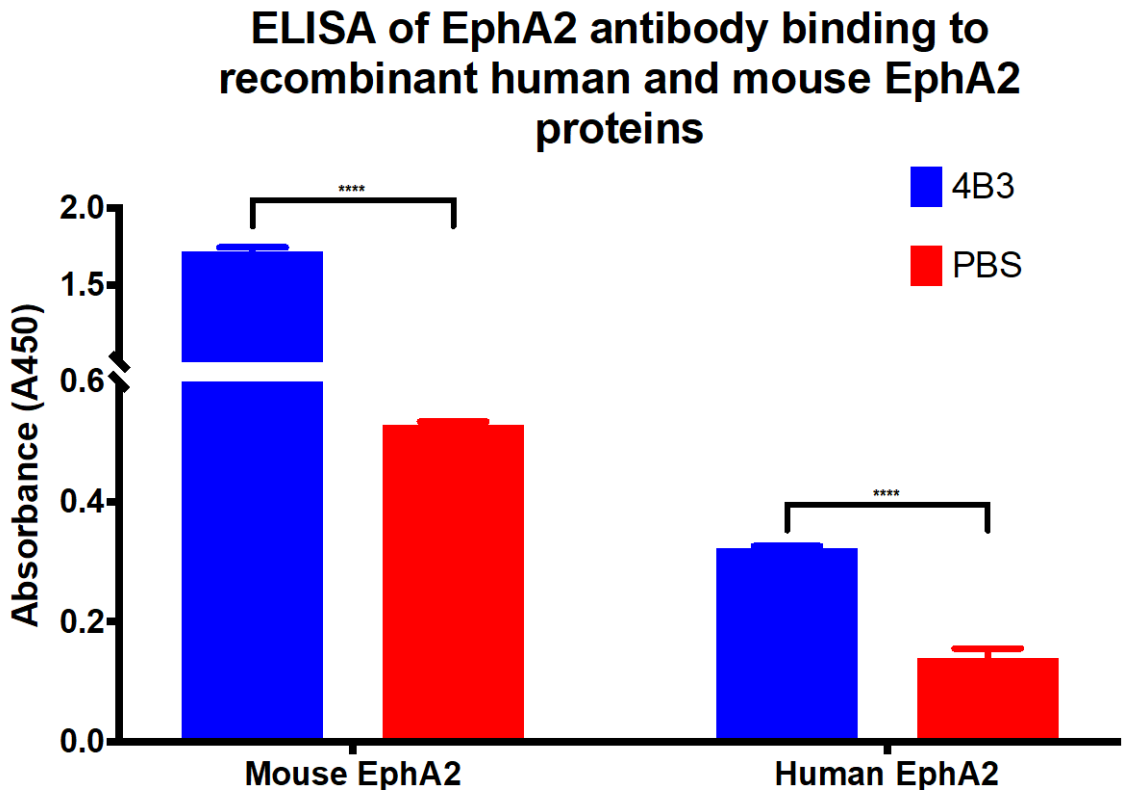

Note: 2 samples (4B3 antibody and PBS) were tested on recombinant mouse and human EphA2 (RnD Systems) coated wells (n=3, each) and then binding detected using a horseradish peroxidase (HRP) labelled anti-mouse antibody (Biorad) that binds 4B3. Binding of the anti-mouse antibody was detected using TMB substrate (Sigma) for HRP and absorbance recorded at A450. Both were found to be statistically significant with respect to PBS as a control ($p<0.0001$ (****) for both)

Section 8 – sNP Characterization

The monomer synthesis and characterization data for all unique compounds are shown below. The polymer was characterized by ^{1}H-NMR (Figure S8.2.1) and dynamic light scattering (DLS, Figure 7.2.2) to determine the properties discussed in the main text. DLS was acquired using a Wyatt Technology DynaPro Plate Reader, with the sample aliquoted into a well of a black-lined 384 well-plate. The sample well contained 20 µL of a 10 mg/mL of sNP in water, and was measured for 20 seconds, with 10 runs. A representative peak is shown from 6 individual samples tested in Figure S8.2.2 with the measurement parameter shown as diameter. A correlogram (Figure S8.2.3) was also acquired and showed a smooth line for each sample, indicating an optimal concentration of the polymer was used. The size of the polymer was found to be 5-10 nm, with no aggregates. Zeta-potential was not possible due to the limitations of the DLS equipment available.

Section 8.1 – Synthesis of NOTA-MA

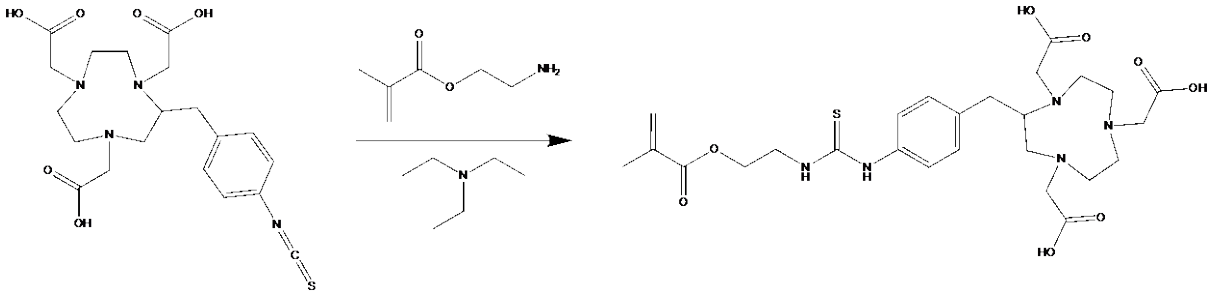

A mixture of 2-aminoethyl methacrylate (5.3 mg, 32.0 µmol) and an excess of TEA (900 µg, 8.83 µmol) was added slowly to a solution of NOTA-NCS (15.0 mg, 26.8 µmol) in DMF (250 µL) at room temperature and allowed to stir for 18h. The reaction mixture was then dried *in vacuo*, reconstituted in MeOH and the filtrate concentrated to give the pure product. Yield 10.2 mg, 66%.^{1}H NMR (500 MHz, DMSO-d_6) δ 10.40 (s, 3H), 10.24 (s, 1H), 8.33 (s, 1H), 7.44 (d, *J* = 8.0 Hz, 2H), 7.28 (d, *J* = 8.0 Hz, 2H), 6.11 (dd, *J* = 1.8, 1.0 Hz, 1H), 5.67 (dd, *J* = 1.8, 1.0 Hz, 1H), 4.27-2.31 (m, 23H), 1.88 (s, 3H) ppm. MALDI-MS for $C_{26}H_{37}N_5O_8S$ (DHBA): calculated $[M + H]^+$ 580.2436, measured $[M + H]^+$ 580.5379.

Figure S8.1.1 – ^{1}H NMR of NOTA-Monomer

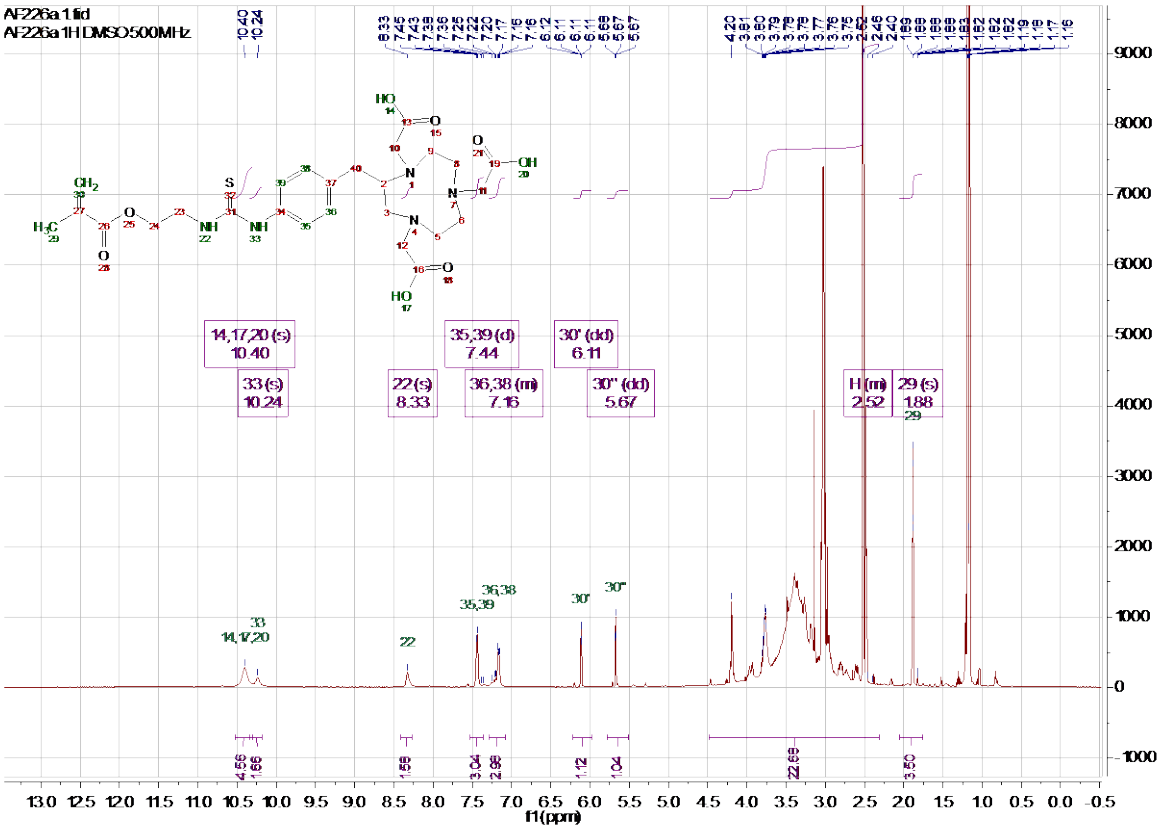

Scheme S8.2 – Characterisation Data for sNP

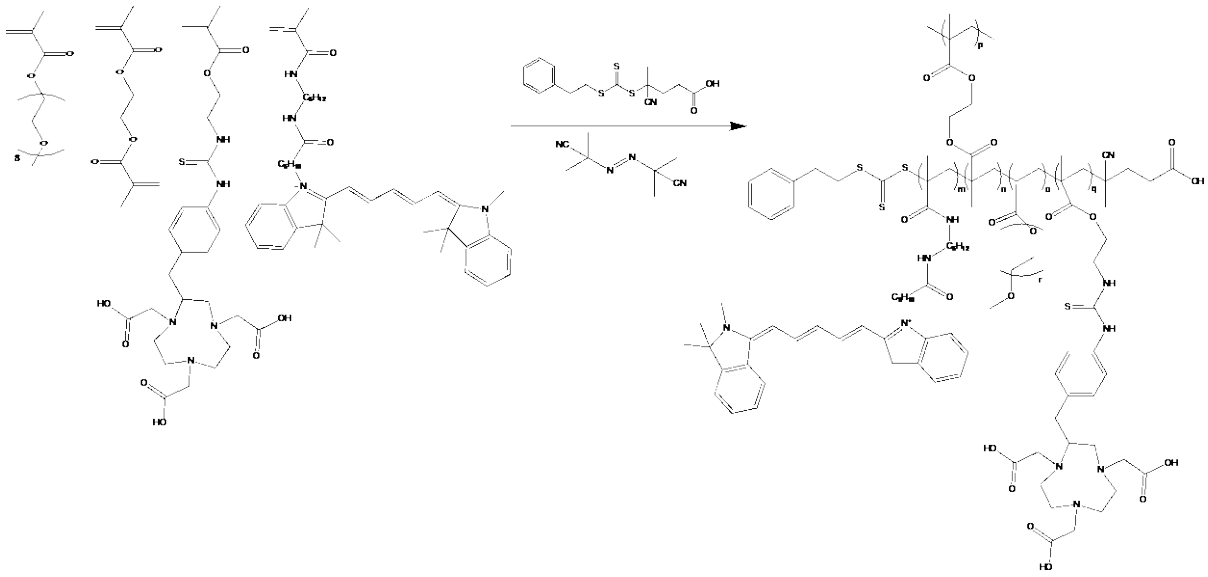

The polymer reported herein was prepared as has been reported previously, but with an acid in place of the pentafluorophenyl end-group and the addition of the afore-described NOTA-MA monomer in place of the tert-butyl carbazate monomer.[5-6] ^{1}H NMR (500 MHz, DMSO-d_6) δ 0.50-2.00 (m, CH_2, CH_3), 3.25-3.75 (m,CH_2CH_2O), 4.02 (s, $COOCH_2$ PEGMA, $COOCH_2$ EGDMA), 7.10-7.30 (m, Ph), 7.22 (d, NOTA-CH), 7.28 (d, NOTA-CH) ppm. Mn ($Đ_M$): 59 kDa (1.6).

Figure S8.2.1 – ^{1}H NMR of sNP

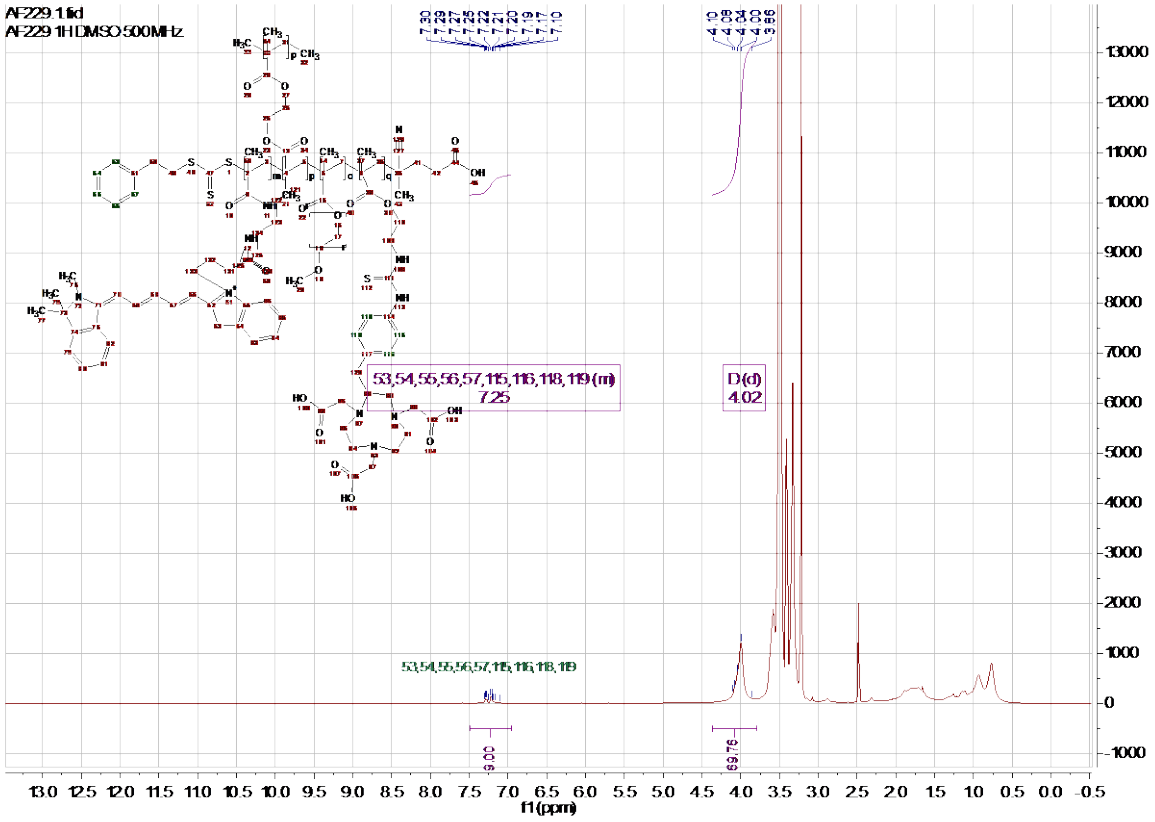

Figure S8.2.2 – Dynamic Light Scattering Size and Aggregation for sNP

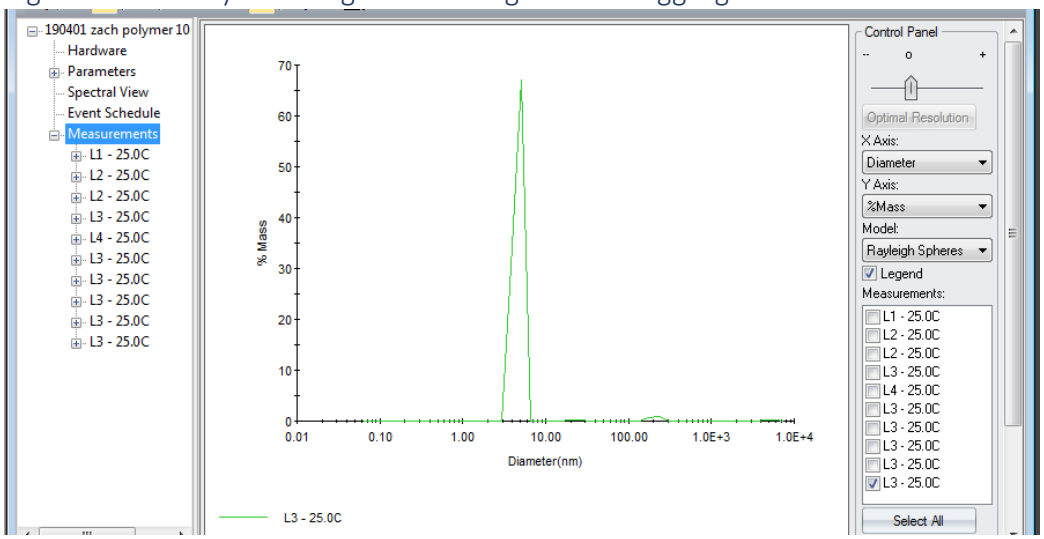

Figure S8.2.3 – Dynamic Light Scattering Correlogram for sNP

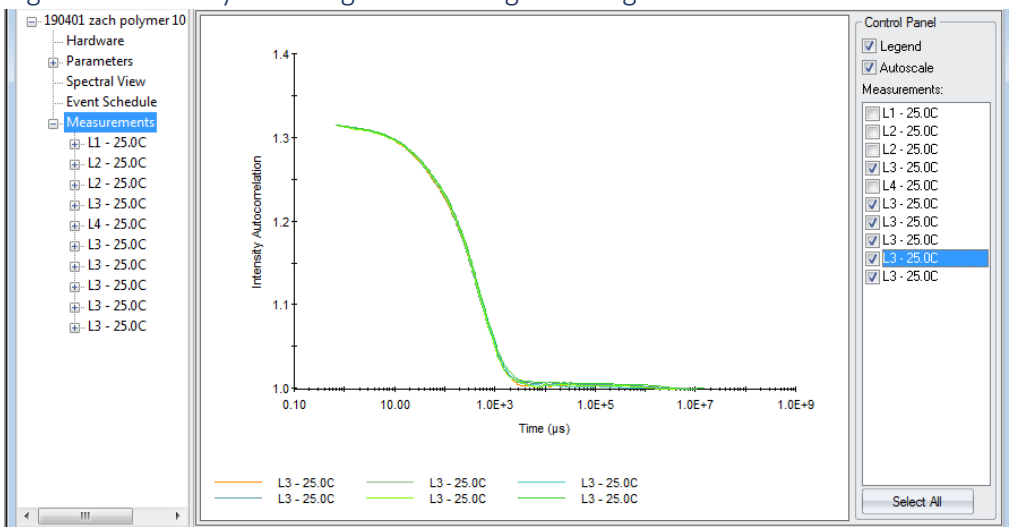

Section 9 – bNP Characterisation

Figure S9.1 – TEM Image of bNP

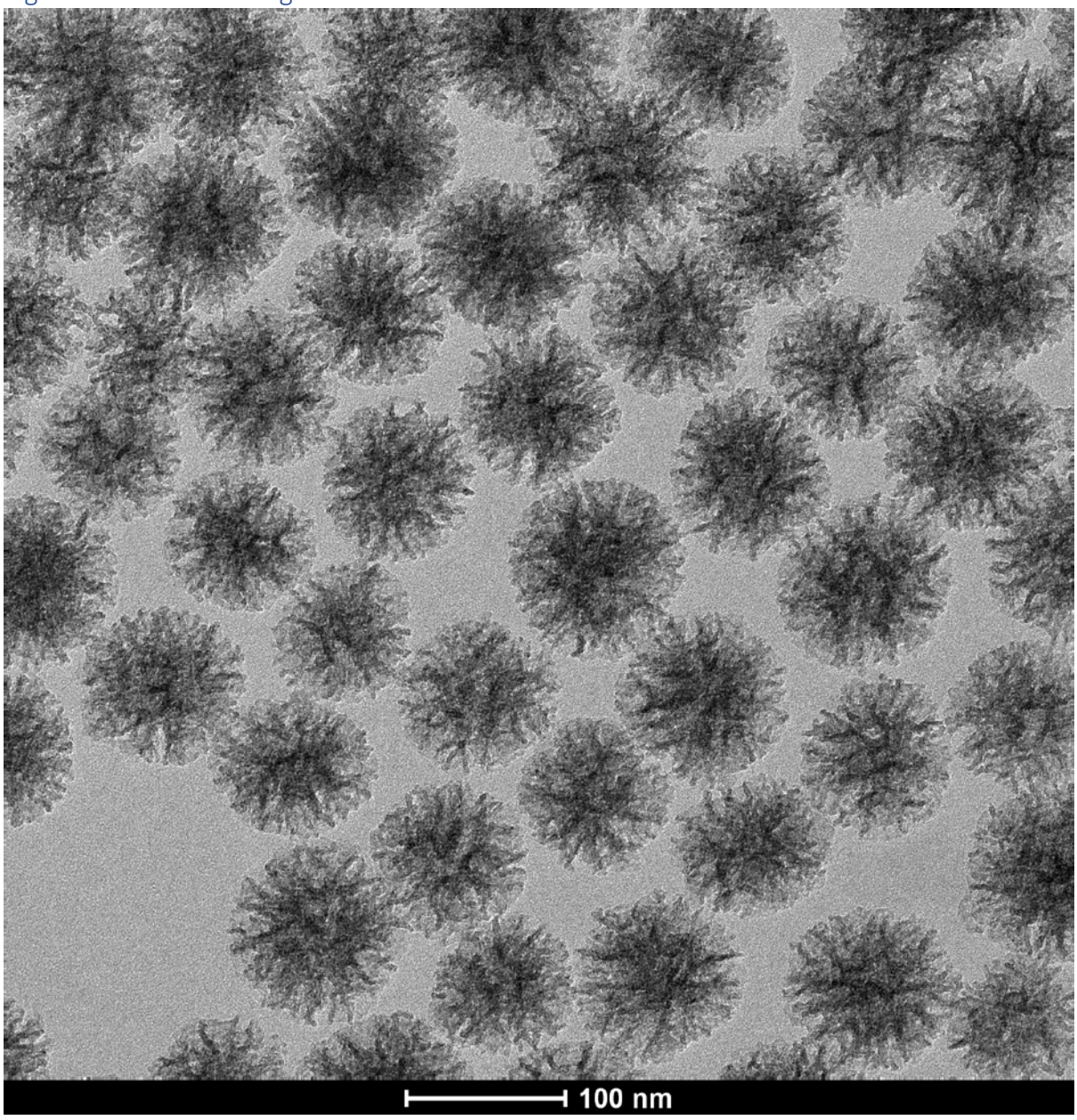

The mesoporous silica particles were sized by TEM (N=100) and found to be 100.8 ± 9.7 nm diameter.

For full characterization data, please see the original publication of these particles.[4, 7]

Section 10 – Minimum Information Reporting in Bio-Nano Experimental Literature (MIRIBEL) Checklist

S10.1 – Checklist Guidelines

The MIRIBEL guidelines were introduced here: https://doi.org/10.1038/S51565-018-0246-4 The development of these guidelines was led by the ARC Centre of Excellence in Convergent Bio-Nano Science and Technology: https://www.cbns.org.au/. Any updates or revisions to this document will be made available here: http://doi.org/10.17605/OSF.IO/SMVTF. This document is made available under a CC-BY 4.0 license: https://creativecommons.org/licenses/by/4.0/.[8]

The MIRIBEL guidelines were developed to facilitate reporting and dissemination of research in bio–nano science. Their development was inspired by various similar efforts:

- MIAME (microarray experiments): *Nat. Genet.* **29** (2001), 365; http://doi.org/10.1038/ng1201-365
- MIRIAM (biochemical models): *Nat. Biotechnol.* **23** (2005) 1509; http://doi.org/10.1038/nbt1156
- MIBBI (biology/biomedicine): *Nat. Biotechnol.* **26** (2008) 889; http://doi.org/10.1038/nbt.1411
- MIGS (genome sequencing): *Nat. Biotechnol.* **26** (2008) 541; http://doi.org/10.1038/nbt1360
- MIQE (quantitative PCR): *Clin. Chem.* **55** (2009) 611; http://doi.org/10.1373/clinchem.2008.112797
- ARRIVE (animal research): *PLOS Biol.* **8** (2010) e1000412; http://doi.org/10.1371/journal.pbio.1000412
- *Nature*'s reporting standards:
    - Life science: https://www.nature.com/authors/policies/reporting.pdf; e.g., *Nat. Nanotechnol.* **9** (2014) 949; http://doi.org/10.1038/nnano.2014.287
    - Solar cells: https://www.nature.com/authors/policies/solarchecklist.pdf; e.g., *Nat. Photonics* **9** (2015) 703; http://doi.org/10.1038/nphoton.2015.233
    - Lasers: https://www.nature.com/authors/policies/laserchecklist.pdf; e.g., *Nat. Photonics* **11** (2017) 139; http://doi.org/10.1038/nphoton.2017.28
- The "TOP guidelines": e.g., *Science* **352** (2016) 1147; http://doi.org/10.1126/science.aag2359

Similar to many of the efforts listed above, the parameters included in this checklist are **not** intended to be definitive requirements; instead they are intended as 'points to be considered', with authors themselves deciding which parameters are—and which are not—appropriate for their specific study.

Table S10.1 - Material characterization

Question	Yes	No
1.1 Are "**best reporting practices**" **available** for the nanomaterial used? For examples, see *Chem. Mater.* **28** (2016) 3535; http://doi.org/10.1021/acs.chemmater.6b01854 and *Chem. Mater.* **29** (2017) 1; http://doi.org/10.1021/acs.chemmater.6b05235		N/A
1.2 If they are available, **are they used**? If not available, ignore this question and proceed to the next one.		
1.3 Are extensive and clear instructions reported detailing all steps of **synthesis** and the resulting **composition** of the nanomaterial? For examples, see *Chem. Mater.* **26** (2014) 1765; http://doi.org/10.1021/cm500632c, and *Chem. Mater.* **26** (2014) 2211; http://doi.org/10.1021/cm5010449. Extensive use of photos, images, and videos are strongly encouraged. For example, see *Chem. Mater.* **28** (2016) 8441; http://doi.org/10.1021/acs.chemmater.6b04639	✓	
1.4 Is the **size** (or **dimensions**, if non-spherical) and **shape of** the nanomaterial reported?	✓	
1.5 Is the **size dispersity** or **aggregation** of the nanomaterial reported?	✓	
1.6 Is the **zeta potential** of the nanomaterial reported?		✓
1.7 Is the **density (mass/volume)** of the nanomaterial reported?		✓
1.8 Is the amount of any **drug loaded** reported? 'Drug' here broadly refers to functional cargos (e.g., proteins, small molecules, nucleic acids).		N/A
1.9 Is the **targeting performance** of the nanomaterial reported, including **amount** of ligand bound to the nanomaterial if the material has been functionalised through addition of targeting ligands?	✓	
1.10 Is the **label signal** per nanomaterial/particle reported? For example, fluorescence signal per particle for fluorescently labelled nanomaterials.		✓
1.11 If a material property not listed here is varied, has it been **quantified**?	✓	
1.12 Were characterizations performed in a **fluid mimicking biological conditions**?		N/A
1.13 Are details of how these parameters were **measured/estimated** provided?	✓	
Explanation for **No** (if needed): 1.6 The zeta potential was not able to be recorded due to incompatibilities between the equipment and material (Cy5 dye) 1.7 Instead of density, the mass of particle was determined and used as a control parameter for cell association study. 1.10 The fluorescent labelling of particles was characterized by fluorescence microscopy images.		

*Ideally, material characterization should be performed in the same biological environment as that in which the study will be conducted. For example, for cell culture studies with nanoparticles, characterization steps would ideally be performed on nanoparticles dispersed in cell culture media. If this is not possible, then characteristics of the dispersant used (e.g., pH, ionic strength) should mimic as much as possible the biological environment being studied.

Table 9.2 – Biological characterization

Question	Yes	No
2.1 Are **cell seeding details**, including **number of cells plated, confluency at start of experiment,** and **time between seeding and experiment** reported?	✓	
2.2 If a standardised cell line is used, are the **designation and source** provided?	✓	
2.3 Is the **passage number** (total number of times a cell culture has been subcultured) known and reported?	✓	
2.4 Is the last instance of **verification of cell line** reported? If no verification has been performed, is the time passed and passage number since acquisition from trusted source (e.g., ATCC or ECACC) reported? For information, see *Science* **347** (2015) 938; http://doi.org/10.1126/science.347.6225.938		✓
2.5 Are the results from **mycoplasma testing** of cell cultures reported?	✓	
2.6 Is the **background signal of cells/tissue** reported? (E.g., the fluorescence signal of cells without particles in the case of a flow cytometry experiment.)	✓	
2.7 Are **toxicity studies** provided to demonstrate that the material has the expected toxicity, and that the experimental protocol followed does not?		N/A
2.8 Are details of media preparation (**type of media, serum,** any **added antibiotics**) provided?	✓	
2.9 Is a **justification of the biological model** used provided? For examples for cancer models, see *Cancer Res.* **75** (2015) 4016; http://doi.org/10.1158/0008-5472.CAN-15-1558, and *Mol. Ther.* **20** (2012) 882; http://doi.org/10.1038/mt.2012.73, and *ACS Nano* **11** (2017) 9594; http://doi.org/10.1021/acsnano.7b04855	✓	
2.10 Is characterization of the **biological fluid** (*ex vivo*/*in vitro*) reported? For example, when investigating protein adsorption onto nanoparticles dispersed in blood serum, pertinent aspects of the blood serum should be characterised (e.g., protein concentrations and differences between donors used in study).		N/A
2.11 For **animal experiments**, are the ARRIVE guidelines followed? For details, see *PLOS Biol.* **8** (2010) e1000412; http://doi.org/10.1371/journal.pbio.1000412	✓	

Explanation for **No** (if needed): 2.4 Cells were purchased from ATCC. The passage number is reported.

*For *in vitro* experiments (e.g., cell culture), *ex vivo* experiments (e.g., in blood samples), and *in vivo* experiments (e.g., animal models). The questions above that are appropriate depend on the type of experiment conducted.

Table 9.3 – Experimental details

Question	Yes	No
3.1 For cell culture experiments: are **cell culture dimensions** including **type of well**, **volume of added media**, reported? Are cell types (i.e.; adherent vs suspension) and **orientation** (if non-standard) reported?	✓	
3.2 Is the **dose of material administered** reported? This is typically provided in nanomaterial mass, volume, number, or surface area added. Is sufficient information reported so that regardless of which one is provided, the other dosage metrics can be calculated (i.e. using the dimensions and density of the nanomaterial)?	✓	
3.3 For each type of imaging performed, are details of how **imaging** was performed provided, including details of **shielding, non-uniform image processing**, and any **contrast agents** added?	✓	
3.4 Are details of how the dose was administered provided, including **method of administration, injection location, rate of administration,** and details of **multiple injections**?	✓	
3.5 Is the methodology used to **equalise dosage** provided?	✓	
3.6 Is the **delivered dose** to tissues and/or organs (in vivo) reported, as % injected dose per gram of tissue (%ID g^{-1})?	✓	
3.7 Is **mass of each organ/tissue measured** and **mass of material** reported?		✓
3.8 Are the **signals of cells/tissues with nanomaterials** reported? For instance, for fluorescently labelled nanoparticles, the total number of particles per cell or the fluorescence intensity of particles + cells, at each assessed timepoint.	✓	
3.9 Are **data analysis details**, including **code used** for analysis provided?	✓	

3.10 Is the **raw data** or **distribution of values** underlying the reported results provided? For examples, see *R. Soc. Open Sci.* **3** (2016) 150547; http://doi.org/10.1098/rsos.150547, https://opennessinitiative.org/making-your-data-public/, http://journals.plos.org/plosone/s/data-availability, and https://www.nature.com/sdata/policies/repositories		✓

Explanation for **No** (if needed):

3.7 Mass of each organ was measured and biodistribution is reported as percentage of injected dose per gram of tissue (%ID g^{-1}).

3.10 Flow cytometry gating strategy is reported in Figure S7. Raw data is available upon request.

* The use of protocol repositories (e.g., *Protocol Exchange* http://www.nature.com/protocolexchange/) and published standard methods and protocols (e.g., *Chem. Mater.* **29** (2017) 1; http://doi.org/10.1021/acs.chemmater.6b05235, and *Chem. Mater.* **29** (2017) 475; http://doi.org/10.1021/acs.chemmater.6b05481) are encouraged.

References

1. Ellingson, B. M.; Bendszus, M.; Boxerman, J.; Barboriak, D.; Erickson, B. J.; Smits, M.; Nelson, S. J.; Gerstner, E.; Alexander, B.; Goldmacher, G.; Wick, W.; Vogelbaum, M.; Weller, M.; Galanis, E.; Kalpathy-Cramer, J.; Shankar, L.; Jacobs, P.; Pope, W. B.; Yang, D.; Chung, C.; Knopp, M. V.; Cha, S.; van den Bent, M. J.; Chang, S.; Yung, W. K.; Cloughesy, T. F.; Wen, P. Y.; Gilbert, M. R.; Jumpstarting Brain Tumor Drug Development Coalition Imaging Standardization Steering, C., Consensus recommendations for a standardized Brain Tumor Imaging Protocol in clinical trials. *Neuro Oncol.* **2015,** *17* (9), 1188-98.
2. Alomair, O. I.; Brereton, I. M.; Smith, M. T.; Galloway, G. J.; Kurniawan, N. D., In vivo High Angular Resolution Diffusion-Weighted Imaging of Mouse Brain at 16.4 Tesla. *PLoS One* **2015,** *10* (6), e0130133.
3. Eisenhauer, E. A.; Therasse, P.; Bogaerts, J.; Schwartz, L. H.; Sargent, D.; Ford, R.; Dancey, J.; Arbuck, S.; Gwyther, S.; Mooney, M.; Rubinstein, L.; Shankar, L.; Dodd, L.; Kaplan, R.; Lacombe, D.; Verweij, J., New response evaluation criteria in solid tumours: revised RECIST guideline (version 1.1). *Eur. J. Cancer* **2009,** *45* (2), 228-47.
4. Cui, J.; De Rose, R.; Alt, K.; Alcantara, S.; Paterson, B. M.; Liang, K.; Hu, M.; Richardson, J. J.; Yan, Y.; Jeffery, C. M.; Price, R. I.; Peter, K.; Hagemeyer, C. E.; Donnelly, P. S.; Kent, S. J.; Caruso, F., Engineering poly(ethylene glycol) particles for improved biodistribution. *ACS Nano* **2015,** *9* (2), 1571-80.
5. Fuchs, A. V.; Tse, B. W.; Pearce, A. K.; Yeh, M. C.; Fletcher, N. L.; Huang, S. S.; Heston, W. D.; Whittaker, A. K.; Russell, P. J.; Thurecht, K. J., Evaluation of Polymeric Nanomedicines Targeted to PSMA: Effect of Ligand on Targeting Efficiency. *Biomacromolecules* **2015,** *16* (10), 3235-47.
6. Pearce, A. K.; Fuchs, A. V.; Fletcher, N. L.; Thurecht, K. J., Targeting Nanomedicines to Prostate Cancer: Evaluation of Specificity of Ligands to Two Different Receptors In Vivo. *Pharm. Res.* **2016,** *33* (10), 2388-99.

7. Cui, J.; Ju, Y.; Houston, Z. H.; Glass, J. J.; Fletcher, N. L.; Alcantara, S.; Dai, Q.; Howard, C. B.; Mahler, S. M.; Wheatley, A. K.; De Rose, R.; Brannon, P. T.; Paterson, B. M.; Donnelly, P. S.; Thurecht, K. J.; Caruso, F.; Kent, S. J., Modulating Targeting of Poly(ethylene glycol) Particles to Tumor Cells Using Bispecific Antibodies. *Adv Healthc Mater* **2019,** *8* (9), e1801607.
8. Faria, M.; Bjornmalm, M.; Thurecht, K. J.; Kent, S. J.; Parton, R. G.; Kavallaris, M.; Johnston, A. P. R.; Gooding, J. J.; Corrie, S. R.; Boyd, B. J.; Thordarson, P.; Whittaker, A. K.; Stevens, M. M.; Prestidge, C. A.; Porter, C. J. H.; Parak, W. J.; Davis, T. P.; Crampin, E. J.; Caruso, F., Minimum information reporting in bio-nano experimental literature. *Nat Nanotechnol* **2018,** *13* (9), 777-785.